GL-TR-89-0313

Processing of DMSP Magnetic Data and Its Use in Geomagnetic Field Modeling

J. R. Ridgway
T. J. Sabaka
D. Chinn
R. A. Langel

NASA Goddard Space Flight Center
Greenbelt, MD 20771

November 1989

Scientific Report No. 1

GEOPHYSICS LABORATORY
AIR FORCE SYSTEMS COMMAND
UNITED STATES AIR FORCE
HANSCOM AIR FORCE BASE, MASSACHUSETTS 01731-5000

"This Technical report has been reviewed and is approved for publication"

FREDERICK J. RICH
Contract Manager

NELSON C. MAYNARD
Branch Chief

FOR THE COMMANDER

RITA C. SAGALYN
Division Director

This report has been reviewed by the ESD Public Affairs Office (PA) and is releasable to the National Technical Information Service (NTIS).

Qualified requestors may obtain additional copies from the Defense Technical Information Center. All others should apply to the National Technical Information Service.

If your address has changed, or if you wish to be removed from the mailing list, or if the addressee is no longer employed by your organization, please notify GL/IMA, Hanscom AFB, MA 01731. This will assist us in maintaining a current mailing list.

Do not return copies of this report unless contractual obligations or notices on a specific document requires that it be returned.

Unclassified
SECURITY CLASSIFICATION OF THIS PAGE

REPORT DOCUMENTATION PAGE

1a. REPORT SECURITY CLASSIFICATION Unclassified	1b. RESTRICTIVE MARKINGS
2a. SECURITY CLASSIFICATION AUTHORITY	3. DISTRIBUTION / AVAILABILITY OF REPORT **Approved for public release; Distribution unlimited**
2b. DECLASSIFICATION / DOWNGRADING SCHEDULE	
4. PERFORMING ORGANIZATION REPORT NUMBER(S) NASA Technical Memorandum 100750	5. MONITORING ORGANIZATION REPORT NUMBER(S) GL-TR-89-0313
6a. NAME OF PERFORMING ORGANIZATION NASA Goddard Space Flight Center 6b. OFFICE SYMBOL (*If applicable*)	7a. NAME OF MONITORING ORGANIZATION Geophysics Laboratory
6c. ADDRESS (*City, State, and ZIP Code*) Greenbelt, MD 20771	7b. ADDRESS (*City, State, and ZIP Code*) Hanscom AFB Massachusetts 01731-5000
8a. NAME OF FUNDING / SPONSORING ORGANIZATION National Aeronautics & Space Administration 8b. OFFICE SYMBOL (*If applicable*)	9. PROCUREMENT INSTRUMENT IDENTIFICATION NUMBER MIPR FY7121-89-03758
8c. ADDRESS (*City, State, and ZIP Code*) Washington, DC 20546-0001	10. SOURCE OF FUNDING NUMBERS PROGRAM ELEMENT NO.: 61102F PROJECT NO.: 2311 2311 TASK NO.: G5 G5 WORK UNIT ACCESSION NO.: EA 02
11. TITLE (*Include Security Classification*) Processing of DMSP Magnetic Data and Its Use in Geomagnetic Field Modeling	
12. PERSONAL AUTHOR(S) J.R. Ridgway*; T.J. Sabaka*; D. Chinn*; R. A. Langel	
13a. TYPE OF REPORT Scientific Report #1 13b. TIME COVERED FROM 10/1/87 TO 9/30/89	14. DATE OF REPORT (*Year, Month, Day*) 1989 November 15. PAGE COUNT
16. SUPPLEMENTARY NOTATION * Science Applications Research, Lanham, Maryland	

17. COSATI CODES			18. SUBJECT TERMS (*Continue on reverse if necessary and identify by block number*)
FIELD	GROUP	SUB-GROUP	Magnetometer DMSP Geomagnetism

19. ABSTRACT (*Continue on reverse if necessary and identify by block number*)
The DMSP F-7 satellite is an operational Air Force meteorological satellite which carried a magnetometer for geophysical measurements. The magnetometer was located within the body of the spacecraft in the presence of large spacecraft fields. In addition to stray magnetic fields, the data have inherent position and time inaccuracies. Algorithms were developed to identify and remove time varying magnetic field noise from the data. Techniques developed for Magsat were then modified and used to attempt determination of the spacecraft fields, of any rotation between the magnetometer axes and the spacecraft axes, and of any scale changes within the magnetometer itself. The corrected data were then used to attempt to model the geomagnetic field. This was done in combination with data from Magsat, from the standard magnetic observatories, from aeromagnetic and other survey data, and from DE-2 spacecraft magnetic field data. The results obtained are inconsistent and contradictory. Characterization of the problem is clearest when model coefficients are compared between models with DMSP data only and models with other data types only. In that case the g_1^1 term in the DMSP models is consistently lower in magnitude by 10-25 nT from the trend inferred from models based on other data. Possible causes include:

20. DISTRIBUTION / AVAILABILITY OF ABSTRACT ☐ UNCLASSIFIED/UNLIMITED ☐ SAME AS RPT. ☐ DTIC USERS	21. ABSTRACT SECURITY CLASSIFICATION Unclassified
22a. NAME OF RESPONSIBLE INDIVIDUAL Frederick Rich	22b. TELEPHONE (*Include Area Code*) 22c. OFFICE SYMBOL GL/PHG

DD FORM 1473, 84 MAR — 83 APR edition may be used until exhausted. All other editions are obsolete.

SECURITY CLASSIFICATION OF THIS PAGE
Unclassified

Cont of Block 19:

First, the spacecraft fields may simply be so strong or variable that any correction procedures are destined to fail; Second, in addition to fixed or slowly varying magnetic sources, there may be a substantial amount of soft magnetization on the spacecraft, for which we do not at present know how to correct; Third, the time and position error on the data furnished to Goddard Space Flight Center may result in systematic errors; Fourth, th automated procedure for removing noise from the data may be inadequate and could possibly introduce error into the resulting data. Future DMSP missions can be upgraded in terms of geomagnetic measurements by upgrading the time and position information furnished with data, placing the magnetometer at the end of a boom, upgrading the attitude determination at the magnetometer, and increasing the accuracy of the magnetometer.

Contents

I. Introduction

The DMSP F7 spacecraft was launched on 18 Nov, 1983 into a 98.74 degree inclination orbit, with apogee 844 km altitude and perigee 822 km. (Rich, 1984). The primary purpose of the spacecraft was to obtain tropospheric meteorological data. However, a triaxial fluxgate magnetometer was included on the spacecraft in order to monitor the geophysical environment. This report deals with the examination of these magnetometer data to evaluate their usefulness in describing the earth's core-produced geomagnetic field.

The field is assumed to be curl free and so representable by a potential function in the form of a spherical harmonic series (Langel, 1987)

$$1) \qquad V = a \sum_{n=1}^{n^*} \sum_{m=0}^{n} (a/r)^{n+1}[g_n^m \cos m\phi + h_n^m \sin m\phi] P_n^m(\cos\theta) + a \sum_{n=1}^{n^{**}} \sum_{m=0}^{n} (r/a)^n [q_n^m \cos m\phi + s_n^m \sin m\phi] P_n^m(\cos\theta)$$

where a is the mean radius of the earth (taken to be 6371.2km), r, θ, and ϕ are the standard spherical coordinates, and the $P_n^m(\cos\theta)$ are the Schmidt quasi-normalized form of associated Legendre functions of degree n and order m. The summation involving (a/r) represents sources internal to the satellite orbit, whereas that involving (r/a) represents external sources such as the ring current.

The magnetic field is then given by

$$2) \qquad \mathbf{B} = -\nabla V$$

Theoretically, 1) and 2) hold only if n* and n** go to infinity. The measured internal **B** contains contributions from both the Earth's core and from its crust; n* in 1) is thus chosen so that V represents fields from the core but not the crust. Langel and Estes (1982) concluded that the core field dominates for $n<13$ and the crustal field for $n>15$. The n* chosen for highly accurate measurements, such as from the MAGSAT satellite, usually equals 13, but because the DMSP observations are less accurate, n* does not exceed 11 in any DMSP model.

The DMSP F7 magnetometer was mounted on the satellite body, as opposed to being attached to a boom, because of spacecraft engineering constraints (Rich, 1984). The magnetometer, a triaxial fluxgate, was aligned with the spacecraft X, Y and Z axes, which are defined as follows: X is vertically down, Y is along-track and Z is cross-track. The three sensor units were built by the Schonstedt Instrument Co., Reston, VA, in the 1960s. The electronics unit for the magnetometer was built by the Applied Physics

Laboratory of Johns Hopkins University, Laurel, MD, based on the design of the MAGSAT fluxgate magnetometer.

The magnetometer acquired field measurements at a rate of 20 samples per second. Measurements were in the form of counts, with one count equalling 12 nano-Teslas (nT). According to Rich (1984), the instrument was not intended to survey the main geomagnetic field, so it was not calibrated with high accuracy on the ground, nor recalibrated in orbit.

Because of the close proximity of the magnetometer to on-board electronic instrumentation, its data were contaminated by non-random instrumental noise, with magnitudes of up to several thousand nT. The attitude of the spacecraft was measured to an accuracy of about 0.1 degree, or 360 arc-seconds. While this attitude accuracy is not as good as that obtained with MAGSAT, in principle it is of sufficient accuracy to enable meaningful vector measurements. In the absence of other near-Earth satellite magnetic field data for this time period, and in view of the success of methods used on MAGSAT to solve for spacecraft fields (see section III), it was decided to investigate the possibility of processing the DMSP F7 data to a stage where they may be useful for main field modeling.

The remainder of this report will deal with several topics related to the DMSP data: 1) the processing steps and problems encountered in removing both random and coherent noise from the data, 2) the correction of data offsets and attitude errors using the GSFC main field software (FIT program), 3) the utilization of processed data in modeling the core-produced geomagnetic field, and 4) the evaluation of those models in regards to the usefulness of this type of data for main field studies.

II. Transformation of On-tape Data to Magnetic Readings.

The magnetometer data contained on the basic DMSP data tapes received from the Air Force is in the form of magnetometer counts, which must be converted into field values in nT in order to be useful. Data is arranged on the tape as a header, containing time and position information for each minute of operation, followed by 60 magnetometer readings (1 per second). All times on the data are rounded to the nearest second. All positions on the original Air Force data are expressed in nautical miles, rounded down to the nearest nautical mile. Nautical miles were converted to kilometers (one nautical mile equals about 1.8 km) in subsequent data processing.

Rounding of the time and position introduces an error of unknown magnitude into the data. An estimate of the possible magnitude of this error can be made as follows. The satellite velocity is about 7.4 km/second. A one second time error is therefore equivalent to an along-track position error of 7.4 km. Combined with the possible 1.8 km roundoff

error in position, the total along-track position error may be as much as 9.2 km. These errors are in addition to those due to actual error in the computed ephemerides.

Langel (1976) has estimated the effects of orbit error on near-earth, polar, satellite magnetic field experiments. His results are summarized in Table 1:

Table 1

Component	Maximum gradient (nT/km)			Mean of gradient magnitude (nT/km)		
	Vertical	Along-trk	Cross-trk	Vertical	Along-trk	Cross-trk
B_r	-28.0	-13.3	6.8	14.9	5.3	2.0
$B\theta$	18.0	-6.5	23.4	7.6	3.0	1.7
$B\phi$	8.4	-2.0	23.3	2.6	0.7	2.1
B	-28.0	-6.1	5.7	18.4	2.5	1.6

A position error of 1.8 km in the vertical direction will give maximum field errors of 50.4, 32.4, and 15.12 nT in B_r, $B\theta$, and $B\phi$, respectively. A position error of 1.8 km in the cross-track direction will give maximum errors of 12.24, 42.12, and 42 nT, and an error of 9.2 km along-track will give maximum field errors of 123, 60, and 19 nT in B_r, $B\theta$, and $B\phi$, respectively. It seems probable that the resulting errors are in the 50-150 nT range and that they may be at least partly systematic in nature.

20 readings per second for each of the magnetometer X, Y and Z axes were originally recorded by DMSP, although only readings #1 and #11 were written on the tapes sent to the Geology and Geomagnetism branch at Goddard (See Appendix A for on-tape data formats). For the Goddard main field studies, only the magnetometer reading associated with the header record was utilized. This preserved sufficient data density (one reading per minute) to fully describe the main geomagnetic field.

The magnetometer was calibrated prior to launch at the NASA Goddard Space Flight Center magnetic test chamber with the following results (Rich, 1984):

3) Measurement (nT) = Calibration Matrix (nT/count) * Measurement (counts) + Bias (nT)

$$\begin{array}{l} \text{(radial)} \\ \text{(along-trk)} \\ \text{(cross-trk)} \end{array} \begin{pmatrix} B_x \\ B_y \\ B_z \end{pmatrix} = \begin{pmatrix} 12.1001 & -0.0055 & 0.0193 \\ -0.0247 & 12.1863 & -0.0101 \\ 0.0069 & 0.0232 & 12.1735 \end{pmatrix} * \begin{pmatrix} C_x \\ C_y \\ C_z \end{pmatrix} + \begin{pmatrix} -0.0653 \\ 59.8733 \\ 39.4228 \end{pmatrix}$$

This equation is used to compute the magnetic field in spacecraft coordinates in nT, given a reading in magnetometer counts. However, this calibration does not take into account the field from the spacecraft, which adds greatly to the bias vector. This vector must be determined from in-flight data. Later work using the FIT program (see Field Value corrections) accomplished this, and re-determined the bias vector as: (89nT, 8457nT, -1441nT) for radial, along-track and cross-track measurements, respectively. These values are still somewhat approximate and require small corrections which will be introduced and discussed in sections VIII and IX. In addition, for computational ease, it was decided to redefine the spacecraft system to be compatible with the MAGSAT coordinate system, so that the spacecraft X axis is defined as cross-track, Y is radially down and Z is along-track. The correct transformation of DMSP magnetometer counts to nano-teslas in spacecraft coordinates compatible with MAGSAT is thus:

4) Measurement (nT) = Calibration Matrix (nT/count) * Measurement (counts) + Bias (nT)

$$\begin{array}{l} \text{(cross-trk)} \\ \text{(radial)} \\ \text{(along-trk)} \end{array} \begin{pmatrix} B_x \\ B_y \\ B_z \end{pmatrix} = \begin{pmatrix} 0.0069 & 0.0232 & 12.1735 \\ 12.1001 & -0.0055 & 0.0193 \\ -0.0247 & 12.1863 & -0.0101 \end{pmatrix} * \begin{pmatrix} C_x \\ C_y \\ C_z \end{pmatrix} + \begin{pmatrix} -1441 \\ 89 \\ 8457 \end{pmatrix}$$

All data discussed in the remainder of this report are assumed to have been processed through this equation and have units of nT. The (B_x,B_y,B_z) measurement vector in equation #4 will henceforth have the label **Bspu**, meaning the vector is in MAGSAT spacecraft coordinates and not yet processed through the corrections discussed in section III.

III. Field Value Corrections.

According to Rich (1984), the DMSP magnetometer may be misaligned relative to the spacecraft by as much as 0.5 degree per axis, with the misalignment measured to an accuracy of about 0.1 degree. Also, bending of the spacecraft body may result in further misalignment. In addition, the values of the three magnetic components may be in error by a fixed bias or by a multiplying factor. The FIT program has the capability to solve for corrections in these parameters in conjunction with the least squares main field solution. The theory of this adjustment is as follows (see also Estes, 1983):

The FIT program computes three types of adjustments to vector satellite magnetometer data: 1) A diagonal calibration matrix containing "slope" parameters, which is multiplied times the measured vector to correct for magnetometer drift, 2) a bias correction vector which is subtracted from the measured vector to correct for constant magnitude offsets, and 3) a rotation matrix which is multiplied times the measured vector to correct for angular offsets of the magnetometer from ideal satellite coordinates. These adjustment parameters are applied to the measured uncorrected data in spacecraft coordinates according to the equation:

5) $$\mathbf{Bspc} = \mathbf{TSM} * \mathbf{TCAL} * (\mathbf{Bspu} - \mathbf{bias})$$

where: **Bspu** is the uncorrected measurement vector in spacecraft coordinates, as given in equation 4).
Bspc is the corrected measurement vector in spacecraft coordinates.
bias is a vector of magnetometer bias corrections in addition to those given in equation 4).
TCAL is the calibration correction matrix of slope parameters.
TSM is the rotation correction matrix.

The elements of **bias** are: (BS_1, BS_2, BS_3), where BS_i are component biases derived in the FIT program, with values derived and discussed in sections VIII and IX.

TCAL has elements:
$$\begin{pmatrix} 1/SL_1 & 0 & 0 \\ 0 & 1/SL_2 & 0 \\ 0 & 0 & 1/SL_3 \end{pmatrix}$$

where SL_i are slopes derived in the FIT program. SL_1 and BS_1 are applied to the satellite X axis, SL_2 and BS_2 to satellite Y axis, and SL_3 and BS_3 to the satellite Z axis components.

The elements of TSM[1] are based on three Euler angles (ϵ_x,ϵ_y, and ϵ_z) solved in execution of the FIT program. (Note: In the FIT program, as of 2/28/88, ϵ_x is denoted ϵ_2, ϵ_y is denoted ϵ_1, and ϵ_z is denoted ϵ_3.) Using the notation TSM_{ij}, where i is the matrix row and j the matrix column, these are:

6)
$$
\begin{aligned}
TSM_{11} &= \cos\epsilon_y * \cos\epsilon_z \\
TSM_{12} &= \cos\epsilon_y * \cos\epsilon_x * \sin\epsilon_z + \sin\epsilon_y * \sin\epsilon_x \\
TSM_{13} &= -\cos\epsilon_y * \sin\epsilon_x * \sin\epsilon_z + \sin\epsilon_y * \cos\epsilon_x \\
TSM_{21} &= -\sin\epsilon_z \\
TSM_{22} &= \cos\epsilon_x * \cos\epsilon_z \\
TSM_{23} &= -\sin\epsilon_x * \cos\epsilon_z \\
TSM_{31} &= -\sin\epsilon_y * \cos\epsilon_z \\
TSM_{32} &= \cos\epsilon_y * \sin\epsilon_x - \sin\epsilon_y * \sin\epsilon_z * \cos\epsilon_x \\
TSM_{33} &= \cos\epsilon_y * \cos\epsilon_x + \sin\epsilon_y * \sin\epsilon_x * \sin\epsilon_z
\end{aligned}
$$

The TSM matrix in the FIT program is derived from 3 rotation matrices (denoted R_x, R_y, R_z) in the spacecraft coordinate system. R_x is a left-handed rotation through the angle ϵ_x, about the spacecraft X axis. R_y is a left-handed rotation about the spacecraft Y axis, with angle of rotation ϵ_y. R_z is a right-handed rotation through the angle ϵ_z, about the spacecraft Z axis.

The matrices R_x, R_y and R_z are thus

7)
$$
R_x = \begin{pmatrix} 1 & 0 & 0 \\ 0 & \cos\epsilon_x & -\sin\epsilon_x \\ 0 & \sin\epsilon_x & \cos\epsilon_x \end{pmatrix} \qquad R_y = \begin{pmatrix} \cos\epsilon_y & 0 & \sin\epsilon_y \\ 0 & 1 & 0 \\ -\sin\epsilon_y & 0 & \cos\epsilon_y \end{pmatrix}
$$

$$
R_z = \begin{pmatrix} \cos\epsilon_z & \sin\epsilon_z & 0 \\ -\sin\epsilon_z & \cos\epsilon_z & 0 \\ 0 & 0 & 1 \end{pmatrix}
$$

Rotations provided by R_x, R_y and R_z are illustrated in Figures 1a), b) and c).

TSM is created by rotating about the X axis first, then about Z, then about Y, e.g.,

8)
$$TSM = R_y * R_z * R_x$$

---

1. Matrices TSM and TGS are named to conform to notations used in Estes, 1983.

An older version of the FIT program, documented in Estes (1983), used a different order of rotation, about the Z axis first, about the new X axis second, and finally about the new Z axis. It is now known that this Z-X-Z rotation order fails to adequately resolve the first and third angles when they are large, and so the present order of rotation was instituted, with successful results.

The relation of euler angles ϵ_x, ϵ_y, ϵ_z to "roll, pitch, yaw" notation is dependent on the spacecraft axis designations. For example, since the MAGSAT Z-axis is pointed in its along-track direction, ϵ_z is roll, ϵ_y(radial) is yaw, and ϵ_x(cross track) is pitch.

The FIT program calculates some field quantities in earth-fixed cartesian coordinates. The coordinate origin is at earth's center; the X axis points along 0° longitude; the Y axis points along 90° meridian; and the Z axis points along the geographic north pole. Information is therefore required on the relation between the corrected spacecraft measurement vector, Bspc, and its analog in earth-fixed coordinates Bef, for every data point. This information is contained in transformation matrix TGS:

9) $$Bef = TGS * Bspc$$

The TGS matrix itself is an approximation computed from the formula:

10) $$TGS = \begin{pmatrix} -n_x & -r_x & v_x \\ -n_y & -r_y & v_y \\ -n_z & -r_z & v_z \end{pmatrix}$$

where: $r_x = \cos\phi\cos\lambda$, $r_y = \cos\phi\sin\lambda$, $r_z = \sin\phi$

$n_x = \cos\phi_n\cos\lambda_n$, $n_y = \cos\phi_n\sin\lambda_n$, $n_z = \sin\phi_n$

$v_x = n_y r_z - r_y n_z$, $v_y = n_z r_x - r_z n_x$, $v_z = n_x r_y - r_x n_y$

ϕ, λ, ϕ_n and λ_n are defined as:

ϕ = Geocentric latitude

λ = East longitude

ϕ_n = -8.74°, the inclination of the vector normal to the orbit

$\lambda_n = \lambda \pm \arccos[-\tan(\phi_n)*\tan(\phi)]$, where + is used for a descending orbit (N to S) and - for an ascending orbit.

It should be noted that this equation is not accurate for latitudes greater than about 75°. DMSP data between 75° and 81.26° were therefore not utilised in subsequent analyses. Derivation of this restriction and of the TGS transformation elements themselves may be found in Appendix B.

Combining equations #5 and #9 yields:

11) $\mathbf{B_{ef}} = TGS * TSM * TCAL * (\mathbf{B_{spu}} - \mathbf{bias})$

$\mathbf{B_{spu}}$ and TGS are read or computed from input data, and TSM, TCAL and **bias** are solved for in execution of the FIT program.

IV. Noise Sources in the Magnetic Data.

The DMSP data were examined initially by Rich (1984), who found three sources of magnetic noise. The first two are high frequency sinusoidal signals with periods of 0.576 and 3.456 seconds. These are caused by the rotating X-ray scanner, designated the SSB/S instrument, which is mounted 10 to 15 inches from the magnetometer sensors and generates a small magnetic field. These high frequency noise sources are of magnitude less than about 30 nT and are not a concern in the present study.

The third noise source found by Rich is the operation of the satellite torquing coils. These are turned on for durations of about 4 minutes at various times throughout the DMSP mission. When the coils are on, the magnetic field data is offset by a constant level shift of 3000 to 14,000 nT. This type of noise is screened out by the "gross outlier" criterion for reducing the data (see section VII).

A fourth known noise source consists of fields in the 100 - 150 nT range which result from turning on transmitters and tape recorders when over a tracking station. It is assumed that most data so affected will be eliminated in the various outlier tests described in section VI.

A noise source not discussed by Rich(1984) was discovered by examining orbital plots of residual data, i.e. data which have had a preliminary field model subtracted. These residual data show strong periodic trends with amplitudes of up to 70 nT, after other corrections were applied. An in-depth discussion of this periodic noise and its removal is found in section VII.

V. Observatory and Survey Data used in Modeling.

Data from land-based magnetic observatories and surveys are instrumental in augmenting the satellite data for modeling purposes. Observatories have permanent locations and are useful in measuring the field behavior over an extended time period. They usually measure declination, plus the horizontal and vertical field components, from which X, Y, Z magnetic components (North, East, and Down in a geodetic system) may be derived. The observatory data used in the DMSP studies were obtained from the World Data Center in Boulder, CO. They are annual means of daily measurements, so each falls on a half year (e.g., 1979.5). Since observatory biases (see next section) were solved for, only those stations with at least 3 measured components and 3 years of data were retained.

The time distribution of observatory data used in this study is:

Table 2

Time period	# of stations
1979 - 1980	143
1980 - 1981	151
1982 - 1983	155
1983 - 1984	149
1984 - 1985	140
1985 - 1986	91
1986 - 1987	1

The geographic distribution of observatories is roughly equal to that displayed in Langel et.al. (1988b).

Survey data include aeromagnetic data (Project Magnet and a Caribbean survey) and land data. The Project Magnet data are 3-component vector recordings, the Caribbean data are scalar values only, and the land data may be declination, inclination, horizontal, north (X), east (Y), vertical (Z) or scalar readings. The aeromagnetic data were averaged over a 220 km distance prior to the least-squares fitting procedure, in order to reduce data volume, attenuate crustal anomalies, and obtain an estimate of data quality for data weighting in the fitting procedure. The averaging method is described in detail in Langel et. al. (1988b).

The land data were checked for quality by comparing to a preliminary field model, and assigned an error estimate via a geographic binning procedure (see Langel et. al., 1988a for description of binning process). The data have extensive geographic coverage; the temporal coverage is described in Table 3.

Table 3.

	Magnet data			Caribbean	Land data						
Time	X	Y	Z	B	D	I	H	X	Y	Z	B
1980	---	---	---	---	1285	110	761	---	---	521	159
1981	306	306	306	---	105	13	88	---	---	71	---
1982	436	436	436	---	132	39	88	---	---	68	34
1983	276	276	276	---	105	---	124	---	---	44	60
1984	---	---	---	142	92	---	71	6	7	71	3
1985	---	---	---	---	329	89	151	---	---	105	151
Total	1018	1018	1018	142	2048	251	1283	6	7	880	407

VI. Calibration Procedure

Fluxgate magnetometers are subject to scale and zero-level drifts due to changes in mechanical properties and electronic components. For MAGSAT, these were solved for in flight by comparison with the on-board scalar magnetometer data. Since no scalar magnetometer was available for DMSP, an attempt was made to use data from magnetic observatories as a "standard" against which to calibrate the DMSP data. Calibration is accomplished by solving for the matrix TCAL (see equation #5) in the modeling procedure. In this process the "standard" data constrain the main field solution sufficiently to permit the TCAL solution.

Two methods of calibration were developed, both of which use observatory data. The use of such data in a main field model necessitates taking into account the presence of crustal fields, fixed measurement biases, and any other field not represented by the model. Langel et. al. (1982) accomplished this by designating the sum of such fields B_m, and the measured field at the observatory B. B_m is called the "bias" at a given observatory. B equals $B_m + B_i$, where B_i is the field from the spherical harmonic model.

In the first method of calibration, B_m is determined for each observatory prior to the spherical harmonic solution, under the assumption that the GSFC(12/83) model, epoch 1980, is highly accurate (Langel and Estes, 1985). B_m for any observatory is taken to be the measured annual mean nearest 1980 (generally at 1980.5) minus the field value computed from the GSFC(12/83) model, truncated at degree 10. (For consistency, the truncation level is the same as that used for models derived with DMSP data.) If an observatory has no data for 1980 then the bias is computed at a later year (1981.5 or 1982.5), and that observatory is assigned a larger error estimate in the subsequent spherical harmonic fit.

Once B_m for each observatory is thus obtained, it is assumed to remain constant through time. B_m is then subtracted from measured observatory values around the epoch of the DMSP data being calibrated. The corrected observatory data are then interpolated to the average epoch of the DMSP data and a field model is generated. The DMSP data are assigned a 200nT weight, compared with 5nT for the observatories. In the spherical harmonic solution, satellite biases, Euler angles, and the elements of TCAL are allowed to vary in addition to the main field coefficients, to obtain the calibration constants.

In the second calibration procedure, B_m is solved for simultaneously with the main field coefficients. This solution requires that data from at least three epochs exist for each observatory (Langel et al, 1982). Thus all observatory data from 1980 through the DMSP time period are used, as opposed to using a single epoch of extrapolated data, as in the first procedure. The observatories and DMSP data are given weights based on residuals to previous fits (generally 25 nT for observatories and 40-80 nT for DMSP data). The epoch of the model is set to 1980. Both main field and time terms are computed, along with the DMSP satellite biases, Euler angles and TCAL elements. The GSFC(12/83) information matrix is used as a priori information, which "anchors" the constant solution at 1980. Observatory biases are solved for, i.e. allowed to vary, in this procedure, versus being held fixed in the first procedure.

This second procedure gives calibration results very similar to the first procedure. However, the second procedure is more versatile, since it can be used to calibrate the DMSP data over its entire time span, whereas the first procedure can only be used to calibrate data from a single epoch, since no secular variation is included in the model. Both of the methods rely on the GSFC (12/83) model for determining the observatory biases, with the implicit assumption that it is a highly accurate model and that the biases remain constant over the time span 1980 - 1985.

VII. Automated Processing Procedure for DMSP Data.

Preliminary field modeling

A test model was generated from DMSP data at epoch 1984.04. The g_1^0 term from this model equaled -29,900.4 nT. A model derived from observatory data at the same epoch yielded g_1^0 equal to -29,883.4. The closeness of the two terms suggests the apparent adequacy of the DMSP data for main field modeling. A calibration of the 1984.04 data, using the second procedure described in the previous section, was also executed with the following results: SL1 = 0.9955, SL2 = 0.9996, SL3 = 1.0025. The nearness of these values to unity again suggests that the DMSP magnetometer measured the magnetic field accurately for that selection of data. These results indicated that DMSP data might be useful for main field modeling, in spite

of the large spacecraft fields. All of these studies were conducted using only a few days of data. On the basis of these results, it was decided to proceed with a larger quantity of data.

The preliminary field model was removed from January 14-18 DMSP data to create residual data. Upon examination, these orbits of data showed strong periodicities. A spectral decomposition of the data revealed noise sources with periods equal to the orbit period (100 minutes) and subharmonics of 1/2, 1/3 and 1/4 of the orbit period. Figure 2 displays a typical residual orbit from this time period. The X and Y components most clearly demonstrate this periodic noise. Figure 3 is the associated spectrum. Peaks in the spectrum display these dominant noise periods quite noticeably. As will be seen below, one cause of the periodic noise is the need for adjustment of the Euler angle values in the TSM matrix in equation 5). The other causes of this periodic noise is unknown. The peak-to-peak amplitude of the noise is about 300 nT before Euler angle correction and about 50-70 nT after that correction.

Automated procedure description

A four-step procedure was followed to remove data spikes and periodic noise from the DMSP data. The steps are as follows: 1) Fit a span of DMSP data, covering several days, with a preliminary field model. Subtract the field model to get residual data. Reject data points above 75° absolute latitude, and reject "gross outliers", i.e., residual data with absolute values greater than a specified cutoff. Fit the residual data with a spline function and reject points which deviate more than 2 standard deviations from that function. 2) Add residual data which is not rejected back to the preliminary field model. Then fit a new field model to this data with epoch equal to the average time of that data span. Solve for constant main field coefficients, magnetometer angle adjustments and biases. 3) Correct the original data with the angle and bias solutions. Use the computed field from step #2 to re-create the residual data, and re-do step #1, i.e. reject gross outliers and spline outliers. 4) Fit a Fourier function, which is composed of the 4 dominant noise periods (25 minutes, 33 minutes, 50 minutes and 100 minutes) in a least-squares manner to the residual data. Reject outliers according to the Fourier fit, using the 2σ criterion as for the spline fit. Then subtract the Fourier function from the data. Add the result back to the computed field model from step #2, to create the final, corrected data set.

Step 4) is somewhat ad hoc. Such periodic variations could arise from source corrections we have either overlooked or been unable to apply. For example, comparison of Figures 4a and 4b shows that much of the large periodic oscillation results from unadjusted Euler angles. It both is more meaningful and reliable to correct the euler angles than to remove the variations via the Fourier fit. For this reason the ad hoc Fourier fit correction is applied last.

To reiterate, the four step process corrects the data in several ways: a) It rejects individual bad points according to a field model, b) It rejects points above 75° which have an inaccurate attitude determination, c) It corrects the data with magnetometer rotations and biases solved for in a least-squares fit, d) It rejects points which are outliers to spline and Fourier function fits, and e) It removes periodic noise from the data by subtracting out the Fourier function.

Figure 4 shows the same profile from Figure 2, after it has undergone the data cleaning process. Most of the periodic noise is gone, and the major spikes and outliers have been removed.

Figure 5 is a world-wide distribution plot of 3 days of processed DMSP data. Note that no data exists polewards of ±75° latitude. Also, every orbit contains a no-data zone approximately 15 degrees long. These points have been rejected according to the "gross outlier" criterion, and evidently are positions in the orbit where the torquing coils were turned on.

A diagnostic of the quality of a data set and the geomagnetic model based on that data set is the "spectrum" from that field model. Consider the quantity:

$$13) \qquad R_n = (n+1) \sum_{m=0}^{n} [(g_n^m)^2 + (h_n^m)^2]$$

R_n is the mean-square value over the Earth's surface of the magnetic field intensity produced by harmonics of the n^{th} degree. Models derived from the MAGSAT data are considered to be the nearest to noise-free of all available models. The presence of noise at any degree will increase the value of R_n. Figure 6 shows two such spectra from DMSP models compared with that for a MAGSAT model (Langel and Estes, 1982). The uncorrected DMSP spectrum, from January 14-18 data, begins to deviate from the MAGSAT spectrum at degree 9, whereas the spectrum from corrected data deviates much less, and not until degree 10. This analysis shows that the removal of noise sources results in an improvement of the character of the output field models. It also shows that the DMSP data are considerably noisier than the MAGSAT data, even when corrected.

VIII. Individual Epoch DMSP Field Models

The correction procedure was applied to 15 sub-sets of DMSP data, each containing several days of data. Subset epochs ranged from January, 1984 through November, 1985. Each data set was chosen from a magnetically quiet

period as determined by the world-wide K_p index. Results of step 2, which solves for the field model and magnetometer adjustment parameters, are summarized in Table 4:

Table 4.

Date yrs	g_1^0 nT	g_1^1 nT	h_1^1 nT	ϵ_x deg	ϵ_y deg	ϵ_z deg	BIAS1 nT	BIAS2 nT	BIAS3 nT
84.02	-29895	-1927	5522	-.038	-.449	0.005	12.0	2.6	-1.7
84.05	-29893	-1928	5532	-.065	-.446	0.006	0.2	-.5	1.4
84.21	-29887	-1935	5523	-.114	-.459	-.004	7.8	2.7	-8.7
84.34	-29872	-1925	5516	-.172	-.457	-.013	11.4	-2.0	-12.5
84.47	-29860	-1922	5514	-.138	-.451	-.016	2.4	-7.6	-11.2
84.63	-29866	-1932	5503	-.063	-.474	-.009	-11.9	-12.1	-3.8
84.71	-29866	-1927	5505	-.092	-.478	-.006	-18.4	-9.5	-2.4
85.05	-29857	-1918	5496	-.050	-.496	-.022	-91.2	-56.7	20.0
85.34	-29856	-1910	5492	-.129	-.471	-.013	-91.2	-67.0	4.1
85.45	-29838	-1920	5494	-.125	-.467	-.017	-93.6	-68.3	1.3
85.46	-29843	-1916	5491	-.130	-.472	-.020	-86.7	-65.9	1.3
85.60	-29842	-1915	5495	-.098	-.475	-.009	-100.4	-74.2	4.6
85.75	-29847	-1908	5490	-.074	-.520	0.013	-112.6	-72.3	7.3
85.82	-29843	-1914	5484	-.081	-.511	0.021	-113.1	-63.7	12.8
85.90	-29832	-1905	5489	-.030	-.518	0.032	-110.0	-57.5	25.7

Figures 7a) through 7e) are derived from Table 4. They display solutions for g_1^0, g_1^1, h_1^1, the three Euler angles, and the three biases for each DMSP data set throughout time. The main field coefficients decrease in magnitude with time as expected from earlier models, but the trend is not smooth. This could indicate that the data sub-sets have marginal geographic distribution, or that the DMSP data are not sufficiently stable over time. The Euler angle solutions are fairly consistent, with ϵ_y (yaw) varying slowly from -.44 to -.52 degrees, ϵ_x (pitch) averaging about -.1 degrees and ϵ_z (roll) averaging about zero. The bias values show a noticeable break between September, 1984 and January, 1985, most strongly in X and Y. Biases at January, 1985 depart sharply from the previous bias trend in all three components. This jump is evident in the biases only, and its cause is uncertain. One possible explanation is that on 30 October, 1984, the solar array panel was rotated 90°. This could result in a changed contribution to the bias field from the solar array since both its position and its total current were changed. Another, though less likely, spacecraft change that could contribute to the bias change is that on 7 November, 1984, the skew momentum wheel was reset so that it drew 100 ma less current.

The bias values in Table 4 are part of the value of the vector parameter **bias** to be used in equation 5), i.e. they are a small time dependent correction to be applied in addition to the large bias values of equation 4). A small further correction is derived in section IX.

IX. Field Models Using All DMSP Data.

Final data processing steps

After the DMSP data sub-sets were corrected according to the euler angles and biases in Table 4, they were prepared for field modeling using the entire combined set. Before concatenation, data from each time period were first examined according to 3-hourly K_p indices and hourly DST values. If the K_p index was greater than 2^+ or the average DST value was greater than 10nT or less than -30nT, then that 3 hour section of data was rejected. Next, data from each period were sorted into equal area geographic bins and randomly deleted in each bin until the best approximation to the following distribution was attained: 3 vector (i.e., 3 components each) points per bin for dip-latitudes less than 30 degrees, and 9 scalar points per bin for dip-latitudes greater than 30 degrees. This distribution is based on work done by Lowes and Martin (1987), which indicates that vector data are required at low magnetic latitudes to avoid the "perpendicular error effect", while scalar data at high latitudes are more effective than vector measurements, because they are more accurate, especially in the presence of field-aligned currents.

After binning, the 15 different time periods were merged together into a single file and entered into a format suitable for input into the FIT program. The final data set consisted of 7750 X and Y measurements, 7768 Z data, and 16097 B data.

All of the DMSP data were then calibrated according to the second procedure in section VI. The field model for this calibration was of degree eleven in the constant field, first derivative (secular variation or SV) terms, and second derivative (secular acceleration or SA) terms. The terminology used herein to designate such a model is (N1,N2,N3), where N1 is the degree of expansion of constant spherical harmonic terms, N2 the degree of expansion of first derivative terms and N3 the degree of second derivative terms. The calibration model is thus described as (11,11,11). Note that $N1 \geq N2 \geq N3$. The GSFC(12/83) model was used as a priori information, the epoch was 1980, and the calibration solution included satellite biases, Euler angles, and TCAL elements. In the solution, the Euler angles were negligible, the bias vector equaled (4.8nT, -0.51nT, 0.65nT), and the slope solution equaled: SL1 = 0.99994, SL2 = 0.99960, SL3 = 1.00119.

These calibration results were applied to the data before creation of the final field models, and these are the final corrections to be applied in accord with equation 5). Thus, in equation 5), the value of **bias** is the sum of this bias value and those found in Table 4; the TCAL matrix is derived from these values of SL1, SL2, and SL3; and the TSM matrix is derived from the Euler angles of Table 4 with no additional correction.

Use of DE-2 data in models

The DMSP data were combined in subsequent fits with 3-component and scalar magnetic field data from the Dynamics Explorer 2 (DE-2) spacecraft. A complete description of these data is given in Ridgway (1988), but is summarized here. 19,600 vector DE-2 magnetic observations, between 10/81 and 1/83, were made available to the Geology and Geomagnetism branch, Goddard Space Flight Center. Since the primary mission of DE-2 was to map field-aligned currents at high latitudes, the data were concentrated in polar regions. The data were also not well distributed temporally, being concentrated at epoch 1982.

These problems necessitated implementation of a binning procedure on the data and decimation within the bins, to distribute the data more equally both temporally and geographically. This procedure cut the number of data to 10,600 vector observations, improved the temporal distribution, reduced data concentration at the poles, and improved data quality by rejecting bad points.

The DE-2 magnetometer was boom-mounted, in order to minimize spacecraft fields. Accuracy of the spacecraft attitude determination, however, was only 0.5°-0.7° (Langel et. al., 1988), resulting in bias and rotational offsets in the three magnetic components. Attitude corrections to the data were empirically computed using the FIT software (see section III), which significantly reduced residuals from calculated field models when applied. The DE-2 data were also calibrated to ground observatories in the same manner as the DMSP data. Results from the attitude correction and the calibration are as follows:

Euler angles :	$\epsilon_x = 0.220°$, $\epsilon_y = -0.091°$, $\epsilon_z = 0.411°$
Biases :	$\mathbf{bias_1} = -10.8$nT, $\mathbf{bias_2} = 6.9$nT, $\mathbf{bias_3} = 2.8$nT
Calibration slopes :	$SL_1 = 0.99928$, $SL_2 = 0.99976$, $SL_3 = 1.00011$

(For biases and slopes, along-track = 1, radial = 2, and cross-track = 3)

Application of these corrections improved the data fit to all subsequent geomagnetic field models. The data residuals, relative to the DE-2 field model at 1982 (excluding external field solution), are:

$$\sigma_x = 44 \text{ nT}$$
$$\sigma_y = 55 \text{ nT}$$
$$\sigma_z = 48 \text{ nT}$$
$$\sigma_b = 24 \text{ nT}$$

These results show that the scalar magnitude data (residual σ_b) is fit much better than the vector component data. Later models, whether using DE-2 data alone (see Ridgway, 1988) or DE-2 plus DMSP data (see following section) were generally most successful when utilizing only the scalar DE-2 data.

Initial Models

The first model using all of the DMSP data, called the MODMSDE model, was of degree (11,11,11), meaning main field static terms, linear time terms, and 2nd order time terms up to degree 11. The "M" of MODMSDE stands for MAGSAT a priori information, from the GSFC(12/83) model. The "O" is for observatory annual means extending from 1979.5 through 1985.5. The "DM" is for DMSP data, with vector data at low latitudes and scalar magnitudes above 30° dip latitude. The "S" stands for world-wide survey data of all measurement types, which were weighted with a correlated weight matrix (see Langel et. al., 1989). The "DE" stands for DE-2 data, divided into vector and scalar data just as for the DMSP set. The model was created in steps, in the order of the letters. Also solved for were observatory biases, three external field coefficients of the first order, and the 4 DST multipliers (one for g_1^0, q_1^0, q_1^1 and s_1^1). The model epoch was 1980, and at 1980 the model was heavily constrained by the MAGSAT data, with the other data primarily determining the temporal variation terms.

Examination of secular variation terms

The secular variation results, for MO, MODM, MODMS, and MODMSDE, all of degree (11,11,11) at epochs 1980, 1985, and 1990, are displayed in Table 5:

Table 5.

Model	Epoch	g_1^0	g_1^1	h_1^1	g_2^0	g_2^1	h_2^1
	1980	25.7	6.0	-28.0	-19.8	5.2	-3.3
MO	1985	21.3	9.2	-20.4	-17.0	5.4	-18.4
	1990	17.0	12.4	-12.7	-14.1	5.6	-33.5
	1980	25.2	6.2	-20.48	-17.2	3.9	-9.9
MODM	1985	28.6	8.9	-20.43	-18.7	2.9	-17.3
	1990	32.1	11.7	-20.38	-20.2	1.9	-24.6
	1980	24.4	9.5	-23.3	-16.8	4.6	-8.7
MODMS	1985	29.0	6.3	-18.0	-19.0	2.0	-18.0
	1990	33.7	3.1	-12.8	-21.2	-0.5	-27.4
	1980	25.1	15.2	-19.5	-15.7	3.7	-10.1
MODMSDE	1985	28.5	1.6	-21.3	-19.9	2.8	-16.9
	1990	31.9	-11.9	-23.2	-24.2	2.0	-23.8

The behavior of these models is not consistent. For the MO model, g_1^0 decreases with time, in contrast to MODM, MODMS and MODMSDE, where it increases from 1980 to 1990. For g_1^1, the MO and MODM models are in good agreement, the MODMS is substantially different, and the MODMSDE shows a totally opposite trend. For h_1^1, both MO and MODMS increase over time, at roughly the same rate. In contrast, the MODM h_1^1 remains constant through time, and the MODMSDE decreases.

It was now apparent that the models had problems. Besides the inconsistent secular variation results, it was found that the calculated correlations between the SV and SA coefficients were highly negative, approaching -1. This means that the solution has strong, undesirable interdependences which might also contribute to the discrepant secular variation results. The parameter space was selectively scaled back to (11,10,5), (11,8,5), and (11,8,0) models. Whenever SA terms were included in the solution, high negative correlations with the SV terms invariably resulted. When the models were of degree (11,8,0), most of the high correlations disappeared, indicating that this is near to the maximum parameter space which can be supported by the available data.

The MO model was also examined. It also showed large correlations, although not as high (±0.75), and more scattered in the solution space. These correlations persisted even when the MO solution was cut to a (11,8,0) model, indicating that available observatory data alone are also not sufficient to solve for a model with this size parameter space.

Examination was also made of the secular variation results from the MO(11,8,0), (11,11,0) and MODM(11,10,5) models. g_1^0, g_1^1 and h_1^1 terms for these models are plotted in Figure 8, along with the same coefficients derived from observatory first-difference data from 1940 through 1979. If the new models are valid, they should be consistent with the trend of the first difference plots. The g_1^0 plots generally match the first-difference trend for the MO models. The MODM model is somewhat off of the trend. For g_1^1, both MO (11,10,5) and MO (11,8,0) fall roughly in the expected coefficient range. MO (11,11,0) is somewhat out of the range, and the MODM model is definitely off of the trend. For the h_1^1 plot, all of the MO models and also the MODM model are consistent with the trend of the first-difference coefficients.

Clearly the different $g1^1$ results in Figure 8b are inconsistent. Agreement of the MO(11,8,0) model with the first-difference trend argues, as above, that the observatory data distribution is inadequate. Addition of the DMSP data should, in principal, greatly improve the data distribution and permit solution for more parameters. But clearly the MODM model is in serious disagreement with the first-difference trend. Adding to the confusion is the apparent agreement of the MODM(11,10,5) model with the MO(11,11) model.

To this point DMSP vector data has been utilized. Since vector data is more error-prone than scalar data, it was decided to examine the possibility that at least some of the model problems stemmed from systematic errors in the DMSP vector data.

MOSDMDE (11,8,5) and (11,11,5) scalar models

Errors in magnetometer attitude, either random or systematic, should not affect the measured scalar magnitude. Accordingly, in order to eliminate any effects of strictly attitude errors, in the next series of models only scalar DMSP and DE-2 data were used, in addition to observatories and survey data. The data included 13,121 DMSP data points at an average epoch of 1985, and 5100 DE-2 points with an average epoch equal to 1982.3. The satellite data were added to a base model consisting of MAGSAT a priori, observatory data, and survey data, called MOS. The epoch of both the (11,8,5) and (11,11,5) models is 1980.

In both resulting models the secular acceleration terms again have high correlations with the corresponding secular variation terms. $\dot{g}_1^0$, $\dot{g}_1^1$ and $\dot{h}_1^1$ coefficients for each model are displayed in Figure 9, along with coefficients derived from the first-differences. (For this plot, first-difference coefficients were also generated from 1980-1985, to add to the 1940-1979 data used in Figure 8.) Plotted in Figure 9 are the MO (11,8,5), MOS (11,11,5), and the MOSDM and MOSDMDE (11,8,5) and (11,11,5) models, at epochs 1980 and 1985.

Examination of Figure 9 again focuses attention on $\dot{g}_1^1$. The $\dot{g}_1^0$ and $\dot{h}_1^1$ models are all in reasonable agreement. Models of $\dot{g}_1^1$ also show some sense of internal agreement, but now with a totally unexpected trend. The $\dot{g}_1^1$ coefficient decreases sharply but steadily from 1982 to 1985, both in the first-difference coefficients and in the models utilizing satellite data. Models with observatory and survey data [MO(11,8,5) and MOS(11,11,5)], which have SA terms, show the same trend, though not as pronounced. This is highly unexpected behavior, unless some sort of geomagnetic jerk is in progress.

MOSDMDE (11,11,5,3) models

The possibility of a jerk in the field at 1982 prompted a test of a (11,11,5,3) model, which provides for non-linear fluctuation of the secular variation terms. Only scalar DMSP and DE-2 data were used, as in the previous models. This model was produced despite the high correlations inherent in solving for an overabundance of time terms. Once MOSDM (11,11,5,3) and MOSDMDE (11,11,5,3) models were completed, parameters were also cut back to obtain a MOSDMDE (11,9,5,3) model. This proved to be very similar to the (11,11,5,3) models.

Plots of the secular variation coefficients from these models present no consistent picture. For $\dot{g}_1^0$ and $\dot{g}_2^2$, the models with satellite data are in disagreement with the first-difference trends. For $\dot{h}_1^1$, $\dot{g}_2^0$, $\dot{g}_2^1$ and $\dot{h}_2^1$ the trends are similar, but not exact. The models for $\dot{g}_1^1$ show a decreasing tend after 1980, but the first-difference trend differs significantly from the trend of models with satellite data. Examination of first-difference plots of observatory data showed no conclusive evidence for a "jerk" in this period. However this is not a conclusive result since the time span of available data from most observatories was too short to definitively determine the trend. Our conclusion is that the data available are not adequate to discern the existence of a jerk.

Trends of the spherical harmonic coefficients

We are left with the puzzle of a possibly anomalous behavior of the $\dot{g}_1^1$ coefficient, particularly when DMSP data are combined with observatory and surface data. It is not yet clear that the DMSP data are consistent with the surface data, or that the DMSP data are reliable for geomagnetic field modeling.

Figure 10, which plots the g_1^0, g_1^1, and h_1^1 coefficients, not the derivatives, derived from the IGRF (1970,1975,1980), the DE-2 calibration (1982), and the individual DMSP runs from Table 4, shows more clearly the nature of the problem with the models based on the DMSP data. For the g_1^0 plot (Figure 10A), the DMSP results fall fairly well along the linear trend of the IGRF models. The DE-2 calibration term, at 1982, is slightly high, but not significantly off-trend. The g_1^1 plot (Figure 10B) reveals much more about the DMSP data. All of the g_1^1 coefficients derived from individual DMSP fits are significantly off of the trend of the IGRF models, having a lower magnitude than expected. The DE-2 g_1^1, however, is slightly higher than expected indicating a discrepancy between the two data sets. The h_1^1 term (Figure 10C) apparently varies in a non-linear manner, with both the DE-2 and the DMSP-derived coefficients falling along the general trend of the IGRF models.

Figure 11 allows further examination of the behavior of the computed g_1^1. Figure 11A shows the individual DMSP fits, along with the DE-2 and DMSP calibration models. The DMSP calibration matches the individual DMSP fits very well. It diverges noticeably from the DE-2 calibration. Figure 11B displays the individual DMSP fits along with the (11,9,5,3) MOSDMDE model, the (11,9) MOSDMDE model, and the MOS (11,9) model. This plot shows that the DMSP models depart noticeably from the models based only on observatory and survey data (MOS model). The DMSP data require a lower g_1^1 term. When combining DMSP data with observatory and repeat data, as in the MOSDMDE(11,9,5,3) model, the g_1^1 term must change dramatically with time to accommodate all data types.

X. Conclusions

The DMSP body-mounted magnetometer data, recorded between 1984 and 1986, have been examined for their utility in geomagnetic field modeling. The data contain major sources of error, as indicated by large data spikes of up to several thousand nT, periodic noise of several hundred nT, and rotational and bias errors in the magnetometer of up to 0.5 degree and one hundred nT.

The data spikes are corrected by a gross-outlier cutoff relative to a preliminary field model and a spline fit. Periodic noise is removed by fitting the data residuals with a 4-component Fourier series. Magnetometer attitude errors are corrected by solving for rotational offsets using the FIT software, and the biases are similarly corrected. The total magnitude of the data is adjusted by calibrating it against ground observatories.

These corrections improve the data quality, as indicated by residual plots and by power spectra of resultant field models. However, although the field models show magnitudes roughly within the realm of believability, closer inspection reveals basic flaws. Any models using Taylor series time representations give high correlations between the secular variation and secular acceleration parameters. This is true for both vector and field magnitude data. More importantly, the models derived from fits to the individual data sets show significant differences to the trend of previous IGRF models and models derived from DE-2 data. These differences are manifested particularly in the g_1^1 spherical harmonic coefficient. In hindsight, if the plots displayed in Figure 11 had been examined early in the analysis process, much of the confusion over the secular variation results could have been avoided.

Unless further methods are found to correct these discrepancies, it is concluded that the data at present are not suitable for main field modeling. There are several possible reasons for this. First, the spacecraft fields may simply be so strong or variable that any correction procedures are destined to fail. Second, in addition to hard magnetic sources and fixed amplitude variable magnetic sources (such as currents), there may be a substantial amount of soft magnetization on the spacecraft. This would result in induced fields which would vary with time and position, and for which we do not at present know how to correct. Third, the timing and position error on the data furnished to Goddard Space Flight Center may result in systematic errors. Fourth, the automated procedure for removing noise from the data, particularly the removal of Fourier components, may be inadequate and could possibly introduce error into the resulting data.

Nothing can be done about the first and second items in the present data. If further effort were to be expended upon the DMSP F-7 data, it should deal with items three and four. A possible approach would be as follows: a) obtain new data from the AFGL, for the same quiet day periods,

with no round-off in time and position information. b) Eliminate spurious data by plotting all of the data, in short sections (1 or 2 orbits), and hand-selecting data segments which are relatively free from variable spacecraft fields due to equipment being turned on or off. Hopefully this procedure would make the Fourier correction unnecessary.

It is not certain that these procedures would be able to salvage the DMSP F-7 data for main field modeling purposes. However, the exercise of processing the data has been instructive, despite difficulties encountered, and good possibilities exist for use of future data.

If the measurement accuracy can be sufficiently upgraded, future DMSP data could make a significant contribution to main field geomagnetism. This is because the present need is for long-term operational observatory-class measurements. Such data would not only provide operational tools such as field models, navigation charts and submarine magnetic detection baselines, but would provide a research tool desperately needed to probe the nature of the geodynamo, the conductivity of the mantle, and the core/mantle momentum exchange mechanism. Keys to upgrading the data quality are: 1) placing the magnetometer on the end of a boom, 2) upgrading the attitude determination at the magnetometer location, and 3) increasing the accuracy of the magnetometer.

It is our understanding that step 3) has already been taken, at least in part. A boom-mounted magnetometer would significantly reduce periodic noise and bias errors in the data. Combined with more accurate attitude determination, such an addition to the DMSP magnetic measuring capabilities would greatly enhance the usefulness of DMSP data in deriving accurate main field models.

XI. Appendix A: DMSP Data Format

I. Tape parameters

Tape density: 6250 BPI

Logical record length: 75 bytes

Block size: 1875.

Fixed block, ASCII.

II. Data format

The data are arranged as one ephemeris record every minute, followed by 60 magnetometer records (one per second).

A. Ephemeris record

location	format	description
1- 4	I4	Year.
5- 8	I4	Day of year.
9-14	I6	Time of ephemeris, seconds U.T.
15-18	I4	Altitude (nautical miles).
19-28	F10.2	Geographic latitude.
29-38	F10.2	Geographic longitude.
39-48	F10.2	Corrected geomagnetic latitude.
49-58	F10.2	Corrected geomagnetic longitude.
59-68	F10.2	Corrected geomagnetic local time.
69-71	3x	Blank.
72-75	I4	Number of data records following ephemeris (usually = 60).

B. Data record

location	format	description
1- 6	I6	Time of data record (seconds UT).
7-11	5x	Blank.
12-29	3I6	X, Y, Z magnetometer counts for first of 20 samples per second.
30-33	4x	Blank.
34-51	3I6	X, Y, Z magnetometer counts for eleventh of 20 samples per second.
52-55	4x	Blank.
56-75	10I2	Ten data quality flags.

XII. Appendix B: Derivation of DMSP Transformation Matrix, TGS.

For every DMSP magnetic reading, known position information includes the geographic latitude, longitude and altitude of the satellite, and the inclination of the satellite orbit plane. From this information, an operator may be derived which transforms measurements in the local satellite coordinate system to an earth-fixed cartesian coordinate system (Originally derived by D. Chinn of Science Applications Research Inc.).

Figure B1 displays a DMSP satellite orbit superimposed upon rotating Earth-fixed cartesian coordinates. The inclination of the satellite orbit plane with the earth's equatorial plane is 98.74 degrees. A local orthogonal coordinate system may be assigned to the satellite, with one axis pointing along the satellite track, another normal to the satellite track, and a radial axis pointing outwards from the earth-fixed origin. The corresponding unit vectors are $\hat{\mathbf{v}}$, $\hat{\mathbf{n}}$, and $\hat{\mathbf{r}}$, respectively.

The unit radial vector r, in cartesian coordinates, equals:

B1) $$\mathbf{r} = r_x\mathbf{i} + r_y\mathbf{j} + r_z\mathbf{k}$$

where:

B2a) $$r_x = \cos\phi\cos\lambda$$
B2b) $$r_y = \cos\phi\sin\lambda$$
B2c) $$r_z = \sin\phi$$

and where ϕ equals the latitude, λ the longitude of the satellite.

The unit normal vector n may be described in an analogous manner, except that ϕ_n replaces ϕ and λ_n replaces λ in equations B1 and B2. ϕ_n equals a constant -8.74° anywhere on the orbit, while λ_n varies throughout the orbit. λ_n is solved for, given ϕ and λ, by utilizing the fact that r * n equals zero:

B3) $$\cos\phi\sin\lambda\cos\phi_n\sin\lambda_n + \cos\phi\cos\lambda\cos\phi_n\cos\lambda_n + \sin\phi\sin\phi_n = 0.$$

Dividing by $\cos\phi$ and $\cos\phi_n$ and switching tangents to the other side of the equation yields:

B4) $$-\tan\phi\tan\phi_n = \cos\lambda\cos\lambda_n + \sin\lambda\sin\lambda_n.$$

Utilizing the addition formula for cosines yields:

B5) $$-\tan\phi\tan\phi_n = \cos(\lambda - \lambda_n)$$

or:

B6) $\lambda_n = \lambda \mp \arccos(-\tan\phi\tan\phi_n)$ (- for ascending orbit, + for descending orbit).

Once λ_n is solved for, then **r** and **n** are fully determined by B2. **v** is derived from the relation:

B7) $\mathbf{v} = \mathbf{n} \times \mathbf{r}$

The transformation from cartesian (**i**,**j**,**k**) to local (**r**,**n**,**v**) coordinates is thus:

B8)
$$\begin{pmatrix} \mathbf{r} \\ \mathbf{n} \\ \mathbf{v} \end{pmatrix} = \begin{pmatrix} r_x & r_y & r_z \\ n_x & n_y & n_z \\ v_x & v_y & v_z \end{pmatrix} * \begin{pmatrix} \mathbf{i} \\ \mathbf{j} \\ \mathbf{k} \end{pmatrix}$$

The MAGSAT-compatible satellite coordinates (x-cross track, y-radially down, z-along track) correspond to -**n**, -**r**, and **v**, respectively, so that the rotation from cartesian to spacecraft coordinates is thus:

B9)
$$\begin{pmatrix} \mathbf{cross} \\ \mathbf{down} \\ \mathbf{along} \end{pmatrix} = \begin{pmatrix} -n_x & -n_y & -n_z \\ -r_x & -r_y & -r_z \\ v_x & v_y & v_z \end{pmatrix} * \begin{pmatrix} \mathbf{i} \\ \mathbf{j} \\ \mathbf{k} \end{pmatrix}$$

The TGS matrix is a rotation from spacecraft to cartesian coordinates, and so equals the inverse (= transpose for a rotation matrix) of the above equation:

B10)
$$\begin{pmatrix} \mathbf{i} \\ \mathbf{j} \\ \mathbf{k} \end{pmatrix} = \begin{pmatrix} -n_x & -r_x & v_x \\ -n_y & -r_y & v_y \\ -n_z & -r_z & v_z \end{pmatrix} \begin{pmatrix} \mathbf{cross} \\ \mathbf{down} \\ \mathbf{along} \end{pmatrix}$$

---- TGS ----

Accuracy of derivation

The accuracy of the TGS derivation depends strongly on the accuracy of the λ_n value in equation B6). A small error in longitude (λ) determination will propagate to an equal error in λ_n, but an error in latitude (ϕ) will propagate to a larger error in λ_n. This relation is

seen by taking the derivative of λ_n with respect to ϕ:

B11) $d\lambda_n/d\phi = -K/(\cos\phi\sqrt{\cos^2(\phi) - K^2\sin^2(\phi)})$ with $K = \tan(-8.74)$

The relation of $d\lambda_n/d\phi$ to ϕ is as follows:

TABLE B1

ϕ	$d\lambda_n/d\phi$
81.26°	∞
80°	10.4
78°	5.2
76°	3.3
75°	2.8

If ϕ is known to within 0.2°, for instance, then the uncertainty in λ_n would equal 0.56, 0.67, 1.0 and 2.1 at 75°, 76°, 78°, and 80°, respectively. Because of this, it was decided not to accept data above 75° latitude.

Alternative formulation

An alternative approach to defining the TGS matrix could be taken if certain DMSP orbital parameters were available. The following derivation is included for clarity of the meaning of TGS. Consider a typical satellite orbit in fixed inertial space, e.g., Figure B2. The X-Y-Z coordinate system is fixed in inertial space with Z along the Earth's rotation axis and X along the vernal equinox. The vernal equinox is the ascending node of the Earth's orbit around the sun. The epoch of X and Z must be specified. Y is chosen to make a right handed system. For our purposes, consider the plane of the orbit to be fixed in the X-Y-Z system. Define the spacecraft coordinate system, X'-Y'-Z' as follows: X' will be positive in the radial direction, Z' will be normal to the orbit plane, with Y' chosen to make a right handed system. For circular orbits, Y' is along track. The angle of the orbital plane with respect to the equatorial plane is called the inclination, i; the intersection of the orbital plane and the equatorial plane, at the point where the satellite is going north is the ascending node. The angle between X and the ascending node, Ω, is called the right ascension of the ascending node. The satellite position in the orbit is then specified by its angle in the orbit plane, ω, measured from the ascending node.

To transform a vector or position from the X' system to the X system requires a set of three rotations: (1) a rotation, R_1, around the Z' axis through the angle ω; (2) a rotation, R_2, through the angle i around the new X axis (the axis through the ascending node): and, (3) a

rotation, R_3, around the Z axis through the angle Ω. This gives

$$B12) \qquad R_1 = \begin{pmatrix} \cos w & -\sin w & 0 \\ \sin w & \cos w & 0 \\ 0 & 0 & 1 \end{pmatrix}$$

$$B13) \qquad R_2 = \begin{pmatrix} 1 & 0 & 0 \\ 0 & \cos i & -\sin i \\ 0 & \sin i & \cos i \end{pmatrix}$$

$$B14) \qquad R_3 = \begin{pmatrix} \cos\Omega & -\sin\Omega & 0 \\ \sin\Omega & \cos\Omega & 0 \\ 0 & 0 & 1 \end{pmatrix}$$

If $R = R_3R_2R_1$, then

$$\begin{aligned}
R_{11} &= \cos\Omega\cos w - \sin\Omega\cos i\sin w \\
R_{12} &= -\cos\Omega\sin w - \sin\Omega\cos i\cos w \\
R_{13} &= \sin\Omega\sin i \\
R_{21} &= \sin\Omega\cos w + \cos\Omega\cos i\sin w \\
R_{22} &= -\sin\Omega\sin w + \cos\Omega\cos i\cos w \\
R_{23} &= -\cos\Omega\sin i \\
R_{31} &= \sin i\sin w \\
R_{32} &= \cos w\sin i \\
R_{33} &= \cos i
\end{aligned}$$

If the X-Y-Z coordinate system is the true-of-date geocentric inertial system, called Celestial Coordinates, CC, then the transformation to Earth fixed coordinates is as follows. The rotation of the Earth, L, since the reference time of the coordinate system is

B15) L = DFRADY*6.3003881 + DELTDY*0.1720279 + GHA

where DELTDY is the number of days since the reference time of the coordinate system,

DFRADY is the fraction of day

GHA is the Greenwich hour angle at the reference time of the coordinate system.

If the X-Y-Z coordinate vector is denoted $\mathbf{X}$ and the Earth-fixed coordinates, X_e, Y_e, Z_e, are denoted $\mathbf{X}_e$, then $\mathbf{X}_e$ is given by

B16) $$\mathbf{X}_e = T_L\mathbf{X}$$

where

B17) $$T_L = \begin{pmatrix} \cos(L + \lambda) & \sin(L + \lambda) & 0 \\ -\sin(L + \lambda) & \cos(L + \lambda) & 0 \\ 0 & 0 & 1 \end{pmatrix}$$

where λ is the longitude.

To then transfer from the Earth fixed equatorial system, $\mathbf{X}_e$, to the topocentric N-E-V (North, East, Vertical, spherical Earth, geocentric) system, the transformation matrix is given by

B18) $$T_t = \begin{pmatrix} \cos(\phi + \pi/2) & 0 & \sin(\phi + \pi/2) \\ 0 & 1 & 0 \\ -\sin(\phi + \pi/2) & 0 & \cos(\phi + \pi/2) \end{pmatrix}$$

where θ is the geocentric colatitude and $\phi = \pi/2 - \theta$ is the latitude.

Combining results, we then have

B19) $$\mathbf{X}_e = T_L R\mathbf{X}' = Q\mathbf{X}' = Q'\begin{pmatrix} \text{cross} \\ \text{down} \\ \text{along} \end{pmatrix}$$

where $Q = T_L R$ and, in the notation of equations B9) and B10), $\mathbf{X}'$ is the vector (-down, along, -cross), and it is easy to show that

$$\begin{aligned}
Q'_{11} &= -Q_{13} = -\cos(L + \lambda)R_{13} - \sin(L + \lambda)R_{23} \\
Q'_{12} &= -Q_{11} = -\cos(L + \lambda)R_{11} - \sin(L + \lambda)R_{21} \\
Q'_{13} &= Q_{12} = \cos(L + \lambda)R_{12} + \sin(L + \lambda)R_{22} \\
Q'_{21} &= -Q_{23} = \sin(L + \lambda)R_{13} - \cos(L + \lambda)R_{23} \\
Q'_{22} &= -Q_{21} = \sin(L + \lambda)R_{11} - \cos(L + \lambda)R_{21} \\
Q'_{23} &= Q_{22} = -\sin(L + \lambda)R_{12} + \cos(L + \lambda)R_{22} \\
Q'_{31} &= -Q_{33} = -R_{33} \\
Q'_{32} &= -Q_{31} = -R_{31} \\
Q'_{33} &= Q_{32} = R_{32}
\end{aligned}$$

Comparison of B19) with B10) shows that TGS = Q' or that

$r_x = Q_{11}$; $r_y = Q_{21}$; $r_z = Q_{31}$; $n_x = Q_{13}$; $n_y = Q_{23}$; $n_z = Q_{33}$

and that

B20) $\tan\lambda_n = n_y/n_x = Q_{23}/Q_{13} = \cos(\Omega+L+\lambda)/\sin(\Omega-L-\lambda)$.

XIII. References

Estes, R.H., Fit program description and user's guide, version 8305, Business and Technological Systems Inc. report, NASA contract NAS5-26486, 1983.

Langel, R.A., Chapter Four: Main Field, in Geomagnetism, ed. J. Jacobs, Academic Press, London, 1987.

Langel, R.A., Effects of orbit error on satellite magnetic field experiments, GSFC Report X-922-76-124, June, 1976.

Langel, R.A., and R.H. Estes, The near-earth magnetic field at 1980 determined from Magsat data, J. Geophys. Res., 90, 2495 - 2509, 1985.

Langel, R.A., and R.H. Estes, A geomagnetic field spectrum, Geophysical Research Letters, 9, 250-253, 1982.

Langel, R.A., R.H. Estes and G.D. Mead, Some new methods in geomagnetic field modeling applied to the 1960-1980 epoch, J. Geomag. Geoelectr., 34, 327-349, 1982.

Langel, R.A., D.R. Barraclough, D.J. Kerridge, V.P. Golovkov, T.J. Sabaka and R.H. Estes, Definitive IGRF models for 1945,1950,1955, and 1960, J. Geomag. Geoelectr., 40, 645-702, 1988a.

Langel, R.A., J.R. Ridgway, M. Sugiura, and K. Maezawa, The geomagnetic field at 1982 from DE-2 and other magnetic field data, J. Geomag. Geoelectr., 40, 1103-1127, 1988b.

Langel, R.A., T.J. Sabaka and R.H. Estes, Error estimates in geomagnetic field modeling, Journal of Geophysical Research, in press, 1989.

Lowes, F.J. and V.E. Martin, Optimum use of satellite intensity and vector data in modeling the main geomagnetic field, Phys. Earth Planet. Int., 48, 183-192, 1987.

Rich, F.J., Fluxgate Magnetometer (SSM) for the Defense Meteorological Satellite Program (DMSP), Block 5D-2, Flight 7, Air Force Geophysical Laboratory Report, AFGL-TR-84-0225, IP#326, July 1984.ADA155229

Ridgway, J. R., Reduction of DE-2 satellite magnetic field data for modeling the main field of the Earth, Science Applications Research Report, #SAR-NASS-28200-488-1, April, 1988.

XIV. Acknowledgements

The help of Rachel Orem with plotting and data management is greatly appreciated. Helpful comments on the manuscript were received from F. Rich of the Air Force Geophysical Lab. This work was sponsered in part by the DMSP Program Office, Space Division, Los Angeles Air Force Station, CA, under a task for Calibration and Validation of DMSP sensors; and in part by NASA RTOP 676-40-02.

TABLES

Figure Captions

Figure #	Caption
1	Relation of Euler angles to spacecraft coordinate system, describing rotations about the X, Y, and Z axes, respectively. Rotations around X and Y (figures a and b) are left-handed, whereas Z is right-handed.
2	DMSP orbital X, Y, and Z magnetic component data which have had an estimated field model removed, revealing strong periodicities in the residuals. The dashed line is a spline fit to the residuals.
3	Power spectra of X and Y DMSP residual data from Figure 2.
4	Y-component of DMSP data from Figure 2, demonstrating removal of outliers, magnetometer rotation and bias correction, and subtraction of Fourier periodic function. The dashed line is a spline fit to the residuals.
5	World-wide geographic distribution of typical three day sequence of processed DMSP data. Note the absence of data above 75° latitude and the large mid-latitude data gaps where the torquing coils were activated.
6	Geomagnetic field spectra. R_n is the total mean square contribution to the vector field from all harmonics of degree n. The spectra are from field models produced from uncorrected and corrected DMSP data; the Magsat spectrum is included for comparison.
7	Plots of g_1^0, g_1^1, h_1^1, Euler angles, and biases versus time (yrs), for field model solutions from 15 DMSP data sets spanning 1984 - 1986.
8	Plots of $\hat{g}_1^0$, $\hat{g}_1^1$, and $\hat{h}_1^1$ for MO(11,8,0), MO(11,11,0), MO(11,10,5) and MODM(11,10,5) models, at epochs 1980 and 1985. Coefficients derived from observatory first differences from 1940 through 1979 are included for comparison.

9 Plots of g_1^0, g_1^1, and h_1^1 for MO(11,8,5), MOS(11,11,5), and both MOSDM and MOSDMDE(11,8,5) and (11,11,5) models, at epochs 1980 and 1985. First difference coefficients from 1940 through 1985 are included for comparison.

10 Plots of g_1^0, g_1^1 and h_1^1 coefficients for individual DMSP fits, the IGRF 1970, 1975 and 1980 models, and the DE-2 1982 calibration model.

11 Plots of the g_1^1 term for individual DMSP fits. Figure 11A includes the DMSP and DE-2 calibration models for comparison. Figure 11B includes the MODMSDE(11,9) and (11,9,5,3) models, and the MOS(11,9) model for comparison.

B1 Relation of DMSP orbit with local n, r, v coordinates to earth-fixed cartesian coordinates.

B2 Geometry of satellite orbit in inertial space. X-Y-Z is coordinate system with Z along the Earth's rotation axis, X along the vernal equinox, and Y so as to give a right handed system. X'-Y'-Z' is the spacecraft coordinate system with X' radial, Z' normal to the orbit, and Y' so as to give a right handed system. Y' is along track. The inclination is i, Ω is the right ascention of the ascending node, and ω is the angular position of the spacecraft measured from the ascending node.

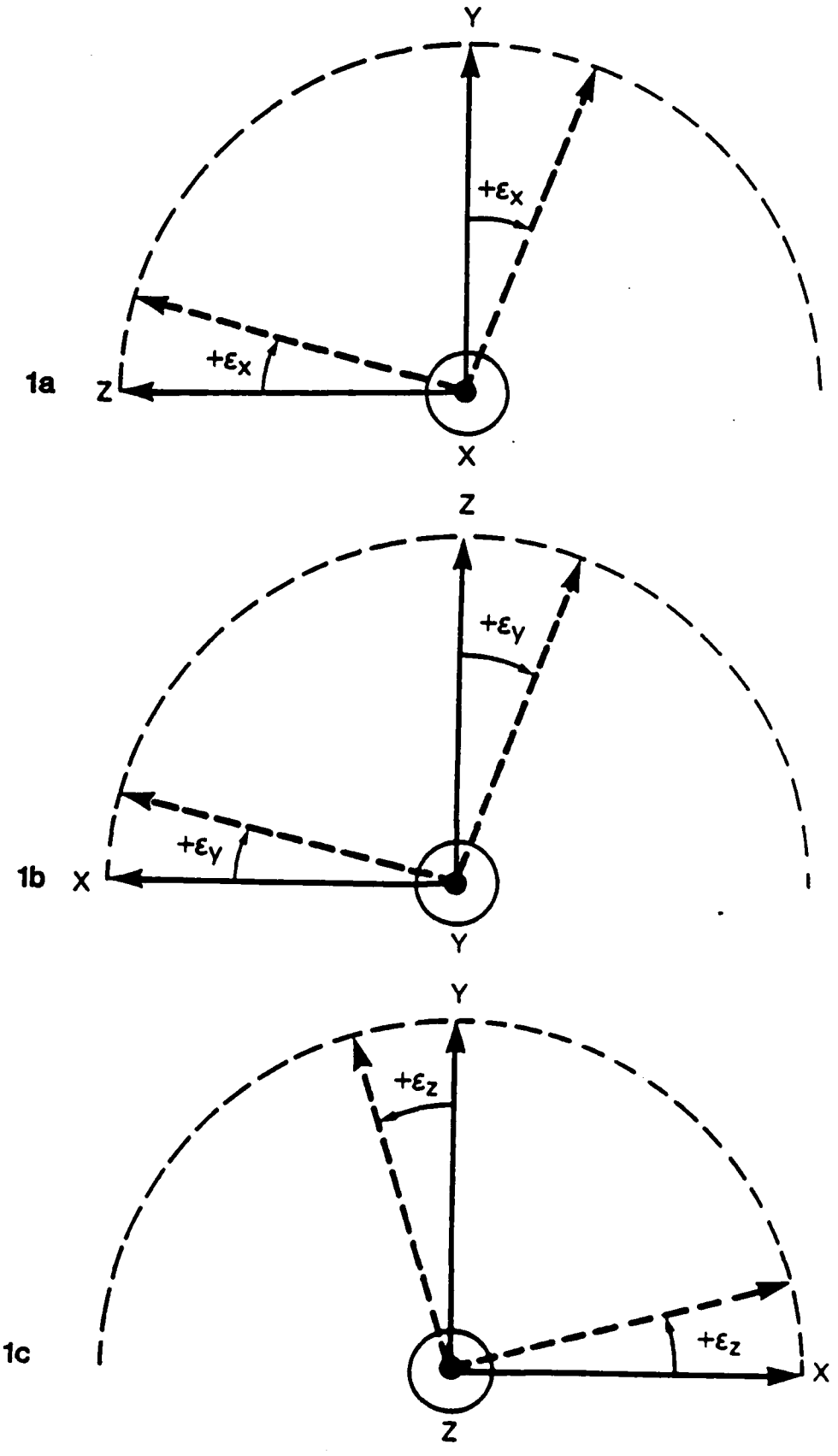

Figure 1

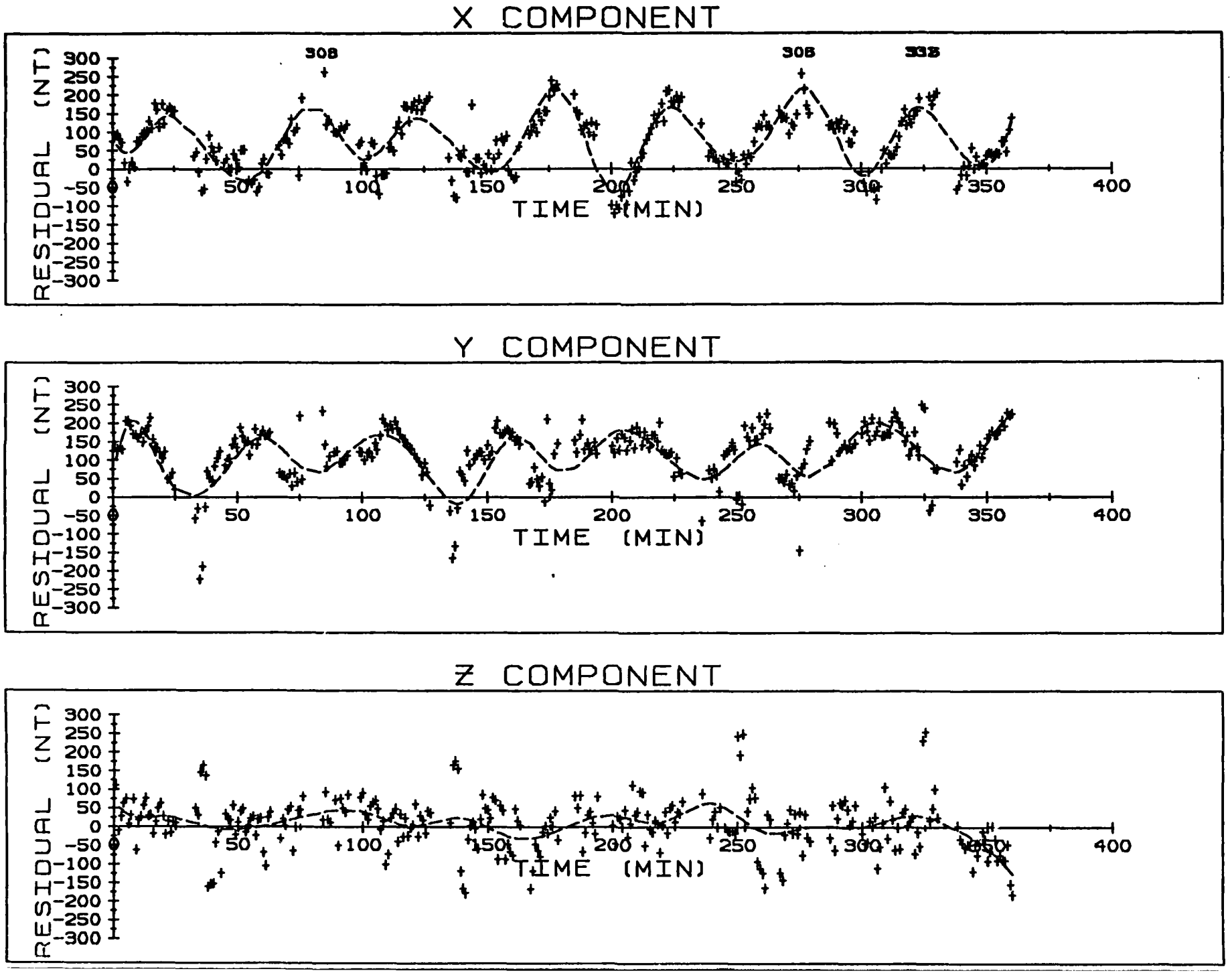
X COMPONENT
RESIDUAL (NT)
300
250
200
150
100
50
0
-50
-100
-150
-200
-250
-300
50
100
150
200
250
300
350
400
TIME (MIN)
Y COMPONENT
RESIDUAL (NT)
TIME (MIN)
Z COMPONENT
RESIDUAL (NT)
TIME (MIN)

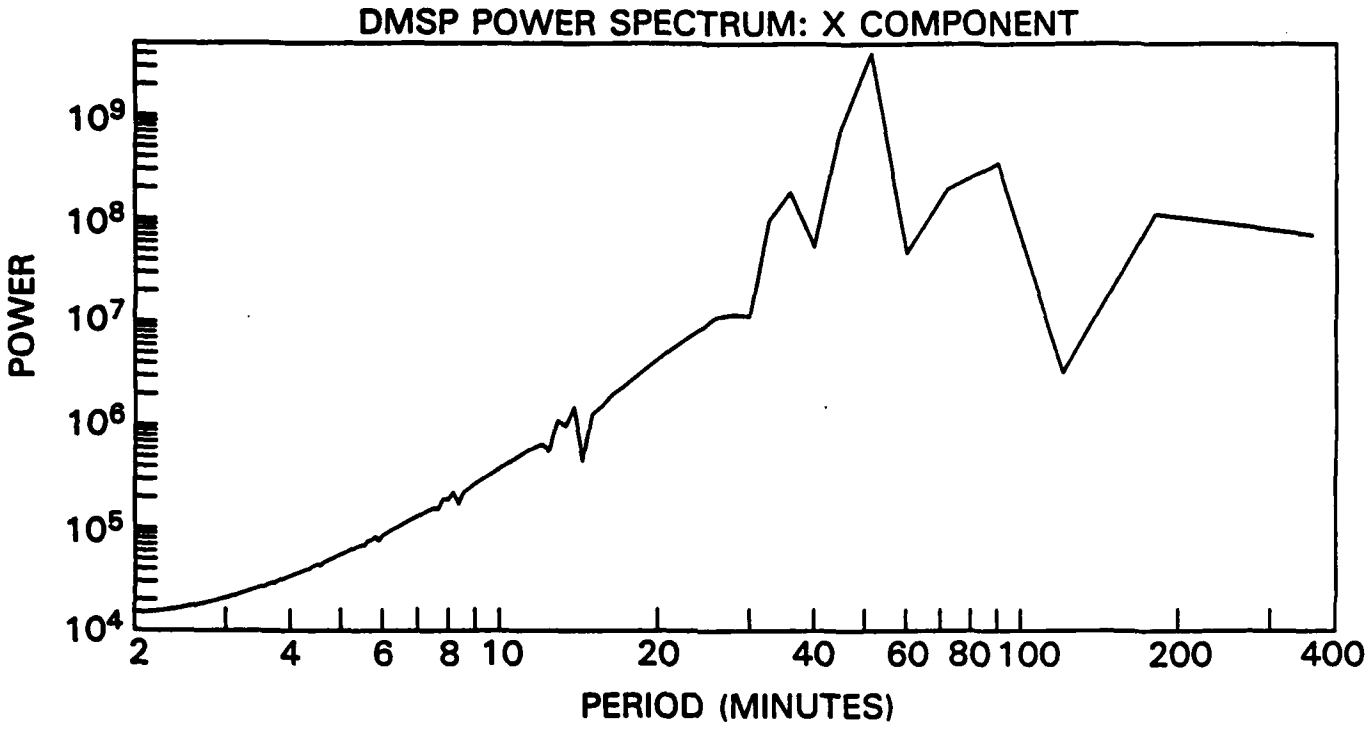
DMSP POWER SPECTRUM: X COMPONENT
POWER
10^9
10^8
10^7
10^6
10^5
10^4
2
4
6
8
10
20
40
60
80
100
200
400
PERIOD (MINUTES)

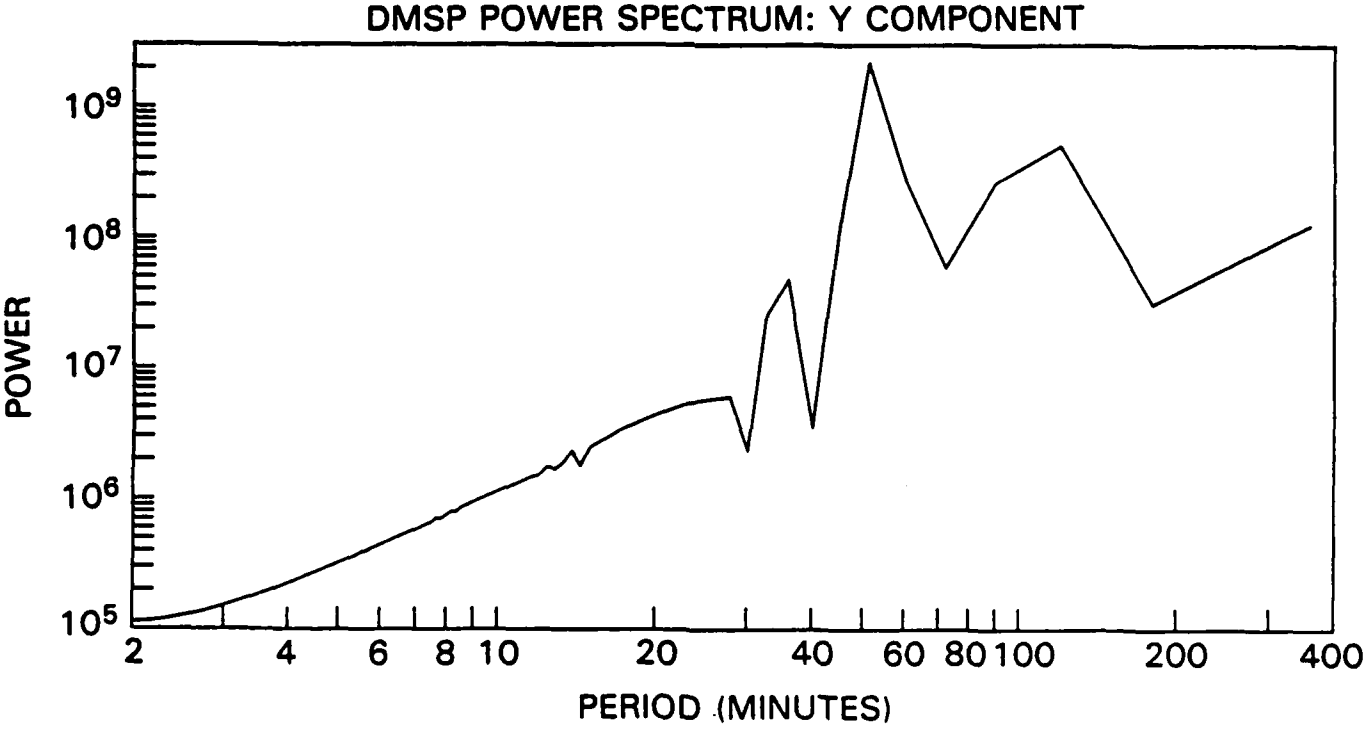
DMSP POWER SPECTRUM: Y COMPONENT
POWER
10^9
10^8
10^7
10^6
10^5
2
4
6
8
10
20
40
60
80
100
200
400
PERIOD (MINUTES)

Figure 3

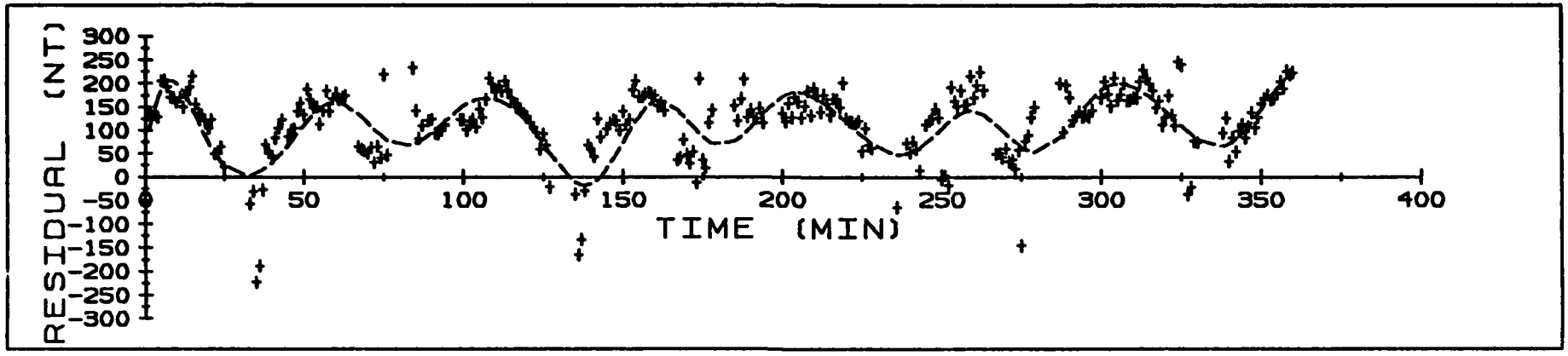
RESIDUAL Y COMPONENT: UNPROCESSED
RESIDUAL (NT)
300
250
200
150
100
50
0
-50
-100
-150
-200
-250
-300
50
100
150
200
250
300
350
400
TIME (MIN)

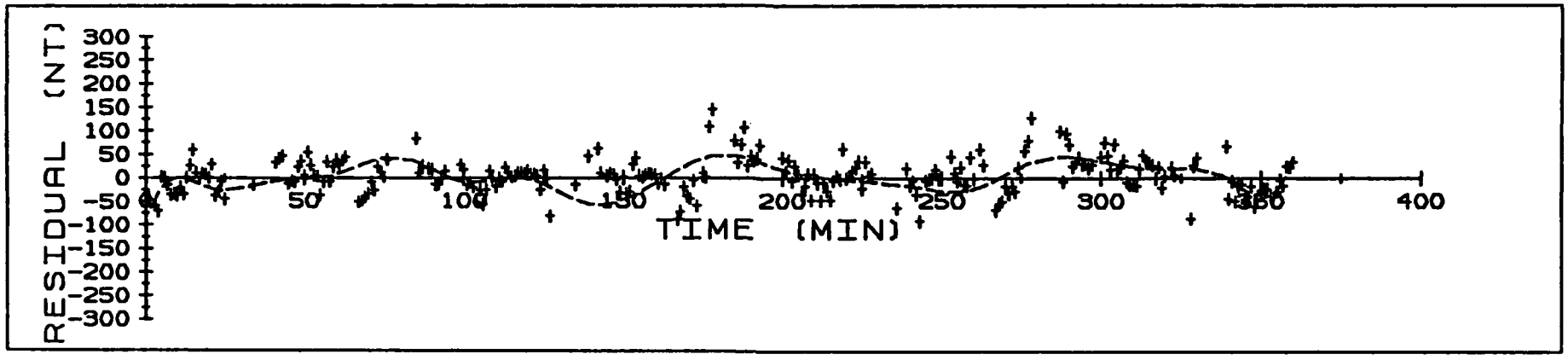
RESIDUAL Y COMPONENT: EULER CORRECTED
RESIDUAL (NT)
300
250
200
150
100
50
0
-50
-100
-150
-200
-250
-300
50
100
150
200
250
300
400
TIME (MIN)

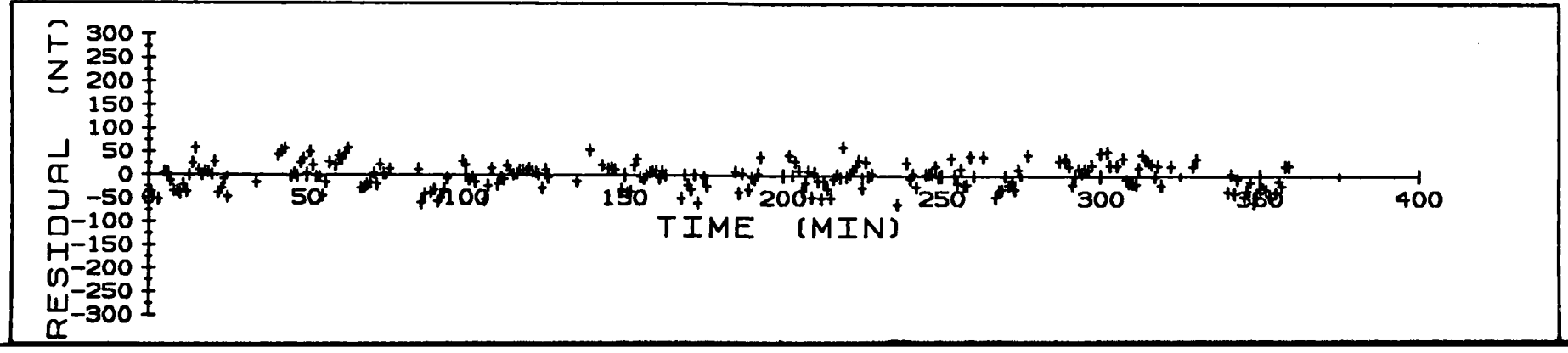
RESIDUAL Y COMPONENT: FOURIER CORRECTED
RESIDUAL (NT)
300
250
200
150
100
50
0
-50
-100
-150
-200
-250
-300
50
100
150
200
250
300
400
TIME (MIN)

DISTRIBUTION OF DMSP DATA: JANUARY 7-9, 1984

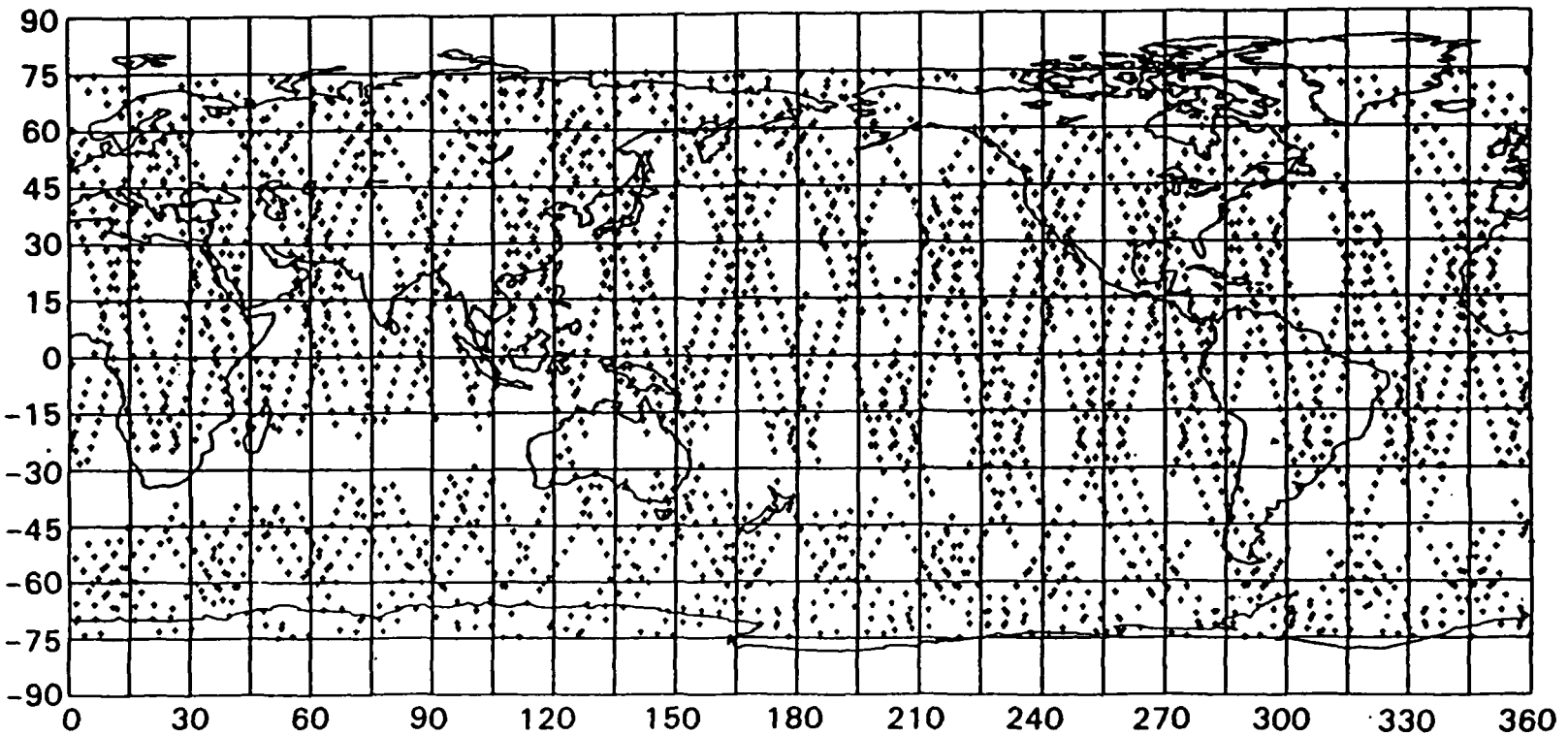

Figure 5

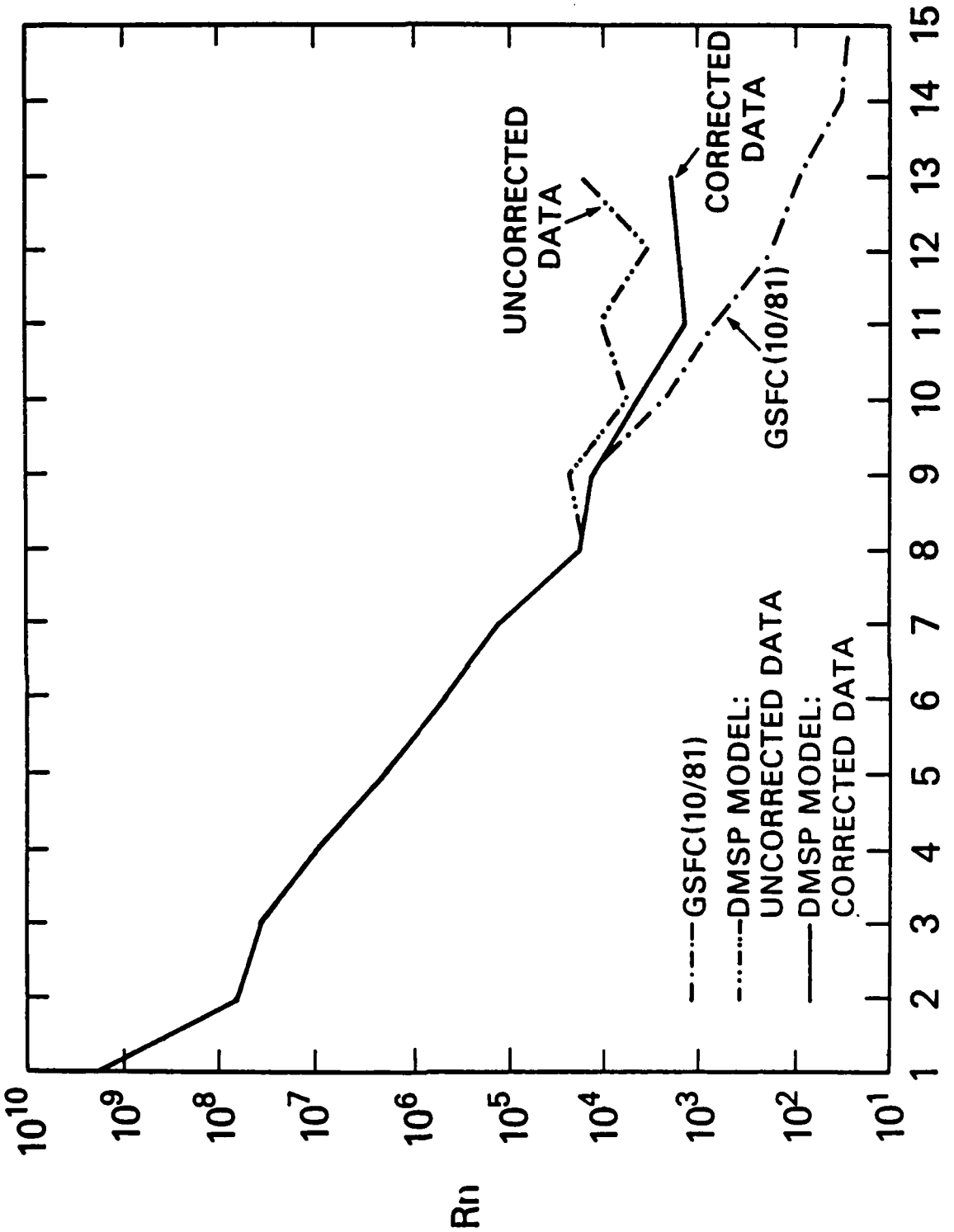
UNCORRECTED DATA
CORRECTED DATA
GSFC(10/81)
GSFC(10/81)
DMSP MODEL: UNCORRECTED DATA
DMSP MODEL: CORRECTED DATA
Rn
DEGREE (n)
10^{10}
10^{9}
10^{8}
10^{7}
10^{6}
10^{5}
10^{4}
10^{3}
10^{2}
10^{1}
1 2 3 4 5 6 7 8 9 10 11 12 13 14 15

Figure 6

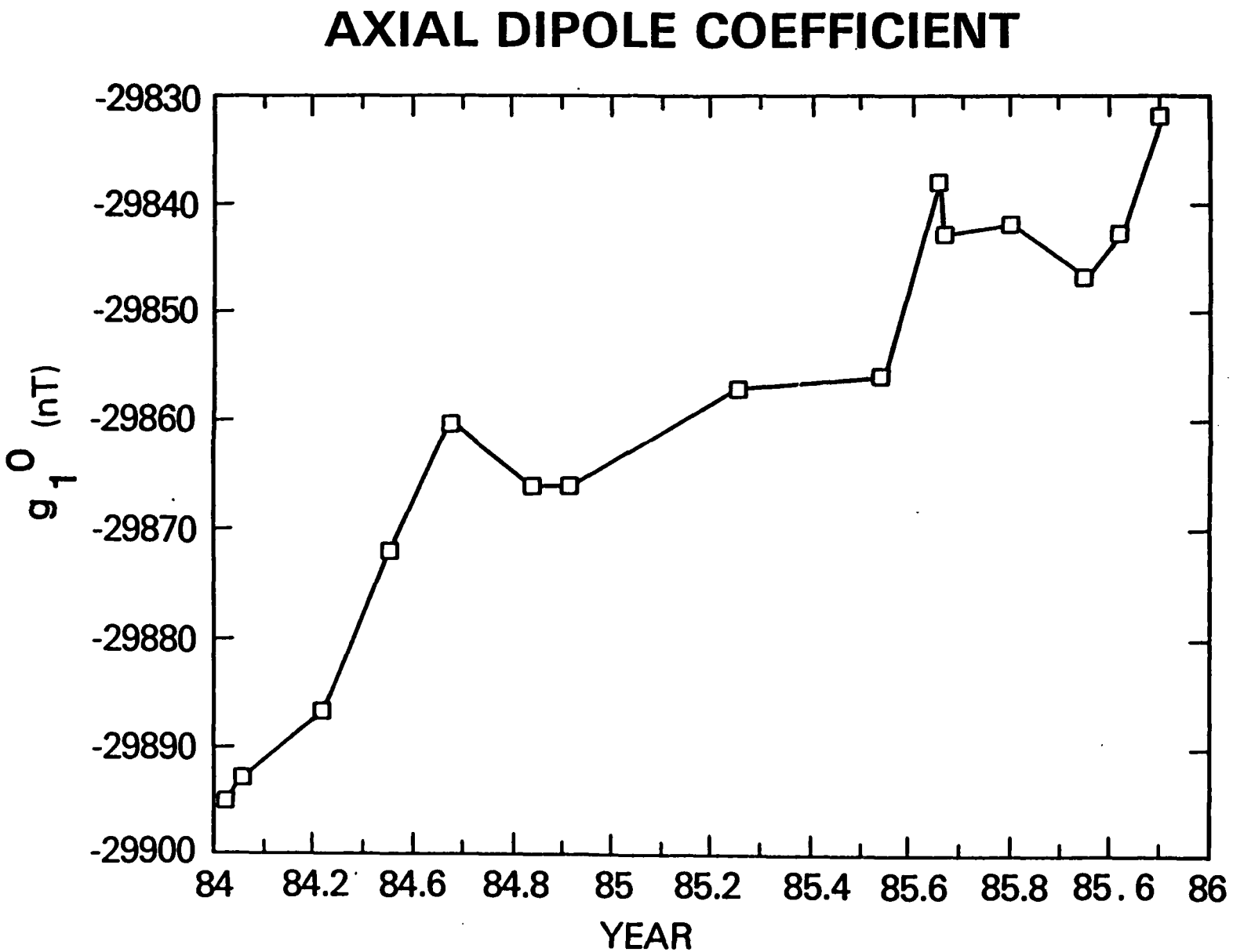
AXIAL DIPOLE COEFFICIENT
-29830
-29840
-29850
-29860
-29870
-29880
-29890
-29900
g_1^0 (nT)
84
84.2
84.6
84.8
85
85.2
85.4
85.6
85.8
85.6
86
YEAR

Figure 7A

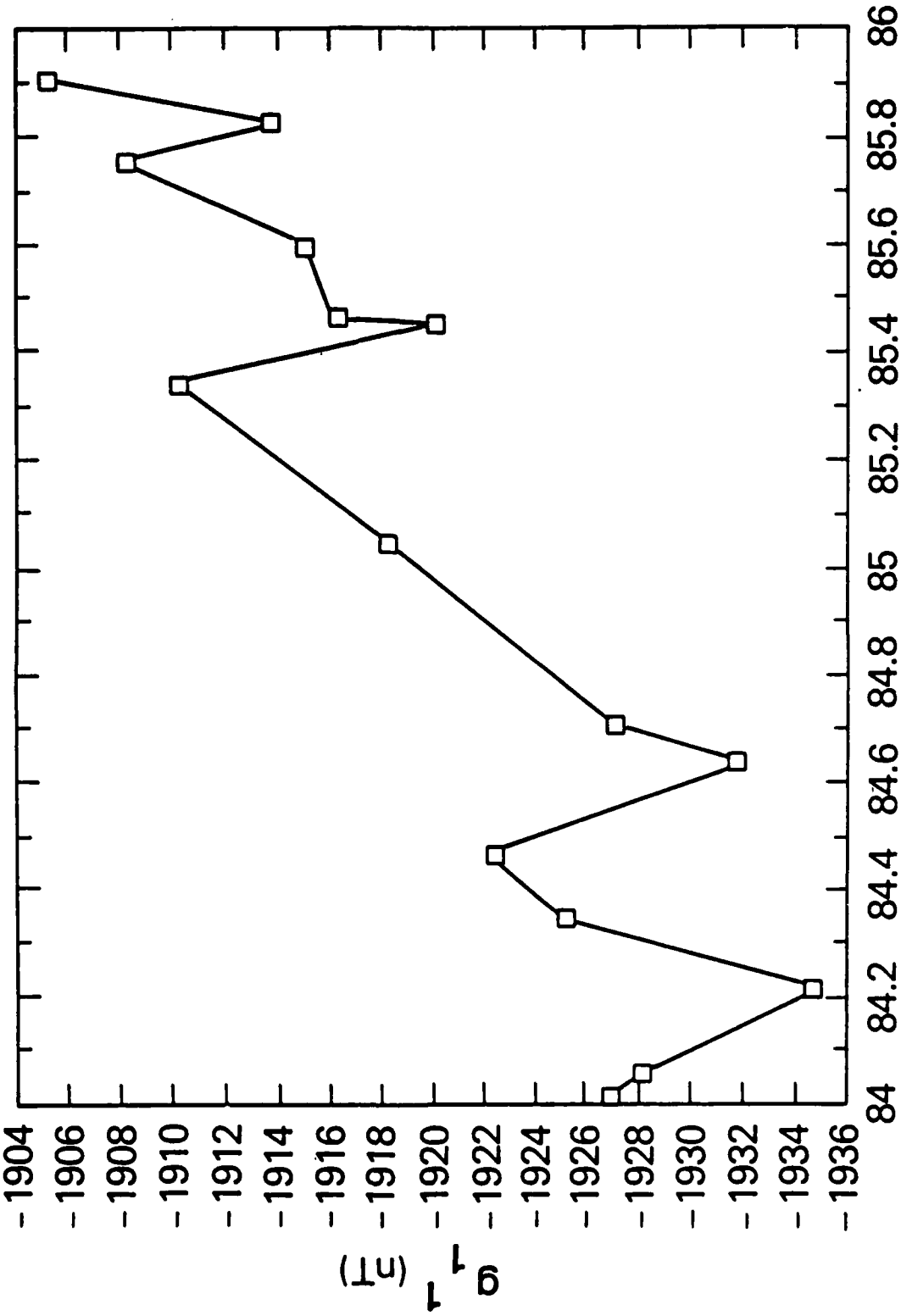
-1904
-1906
-1908
-1910
-1912
-1914
-1916
-1918
-1920
-1922
-1924
-1926
-1928
-1930
-1932
-1934
-1936
g_1^1 (nT)
84
84.2
84.4
84.6
84.8
85
85.2
85.4
85.6
85.8
86
YEAR

Figure 7B

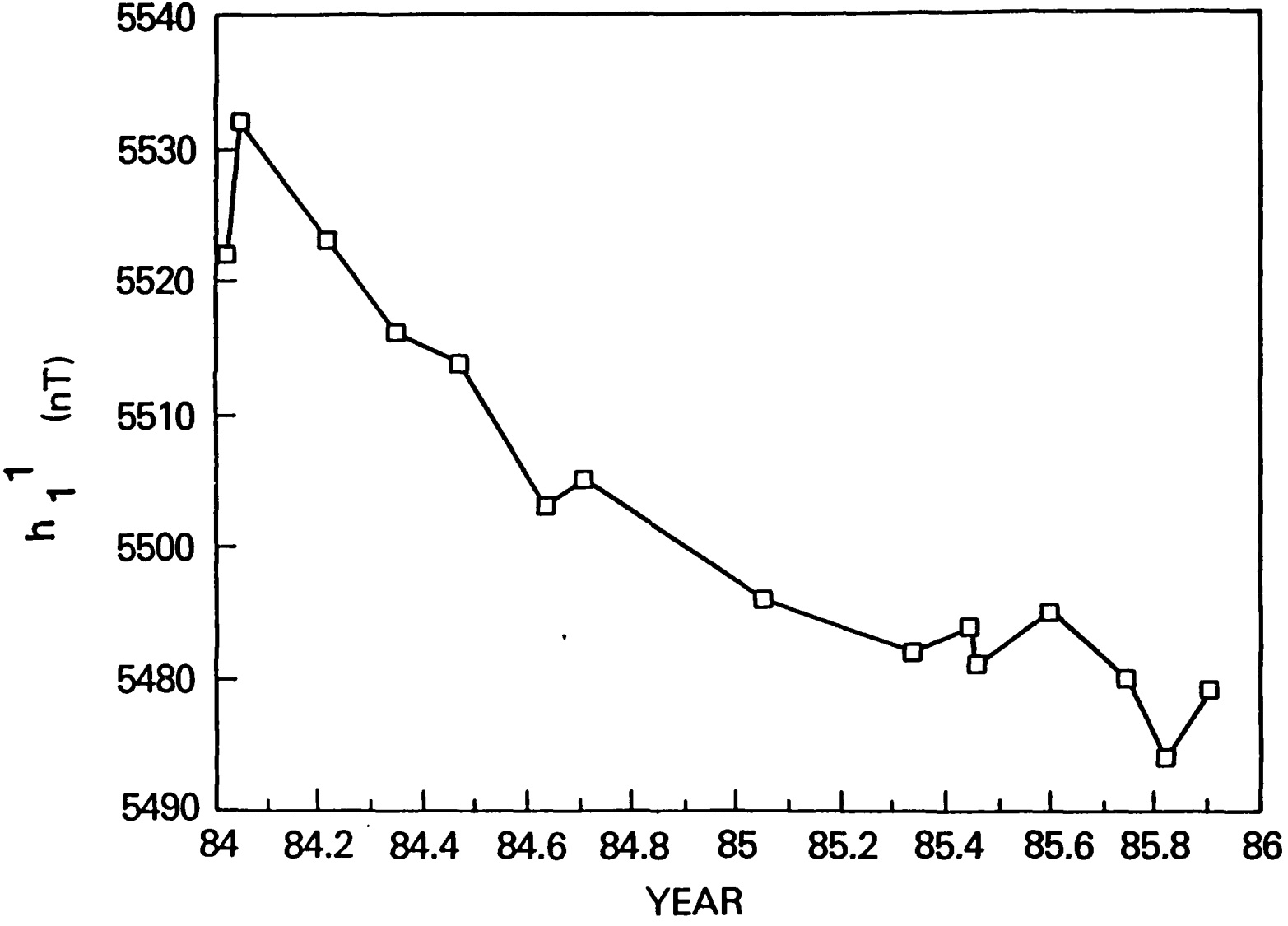
5540
5530
5520
5510
5500
5480
5490
h_1^1 (nT)
84
84.2
84.4
84.6
84.8
85
85.2
85.4
85.6
85.8
86
YEAR

Figure 7C

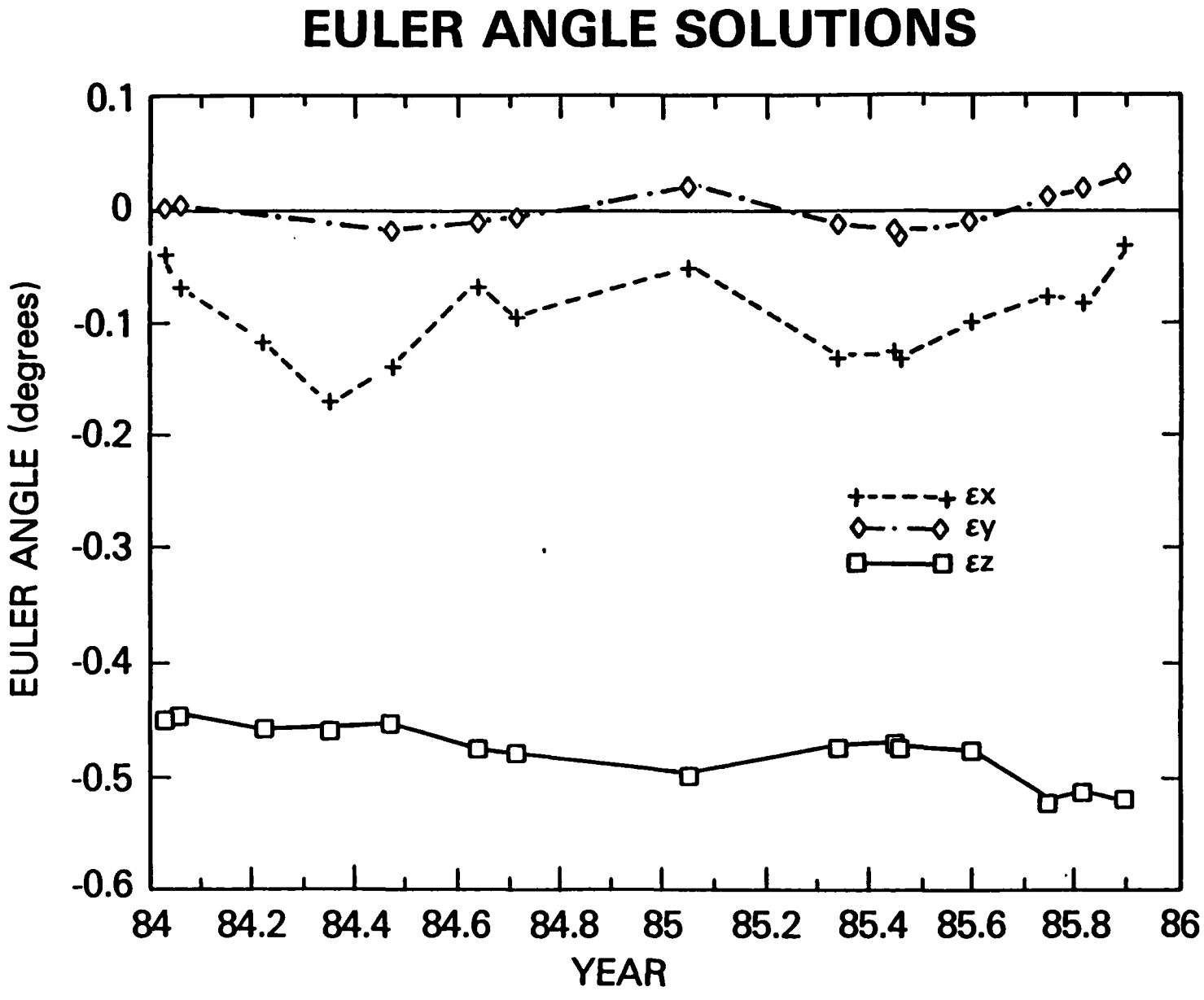
EULER ANGLE SOLUTIONS
EULER ANGLE (degrees)
0.1
0
-0.1
-0.2
-0.3
-0.4
-0.5
-0.6
84
84.2
84.4
84.6
84.8
85
85.2
85.4
85.6
85.8
86
YEAR
εx
εy
εz

Figure 7D

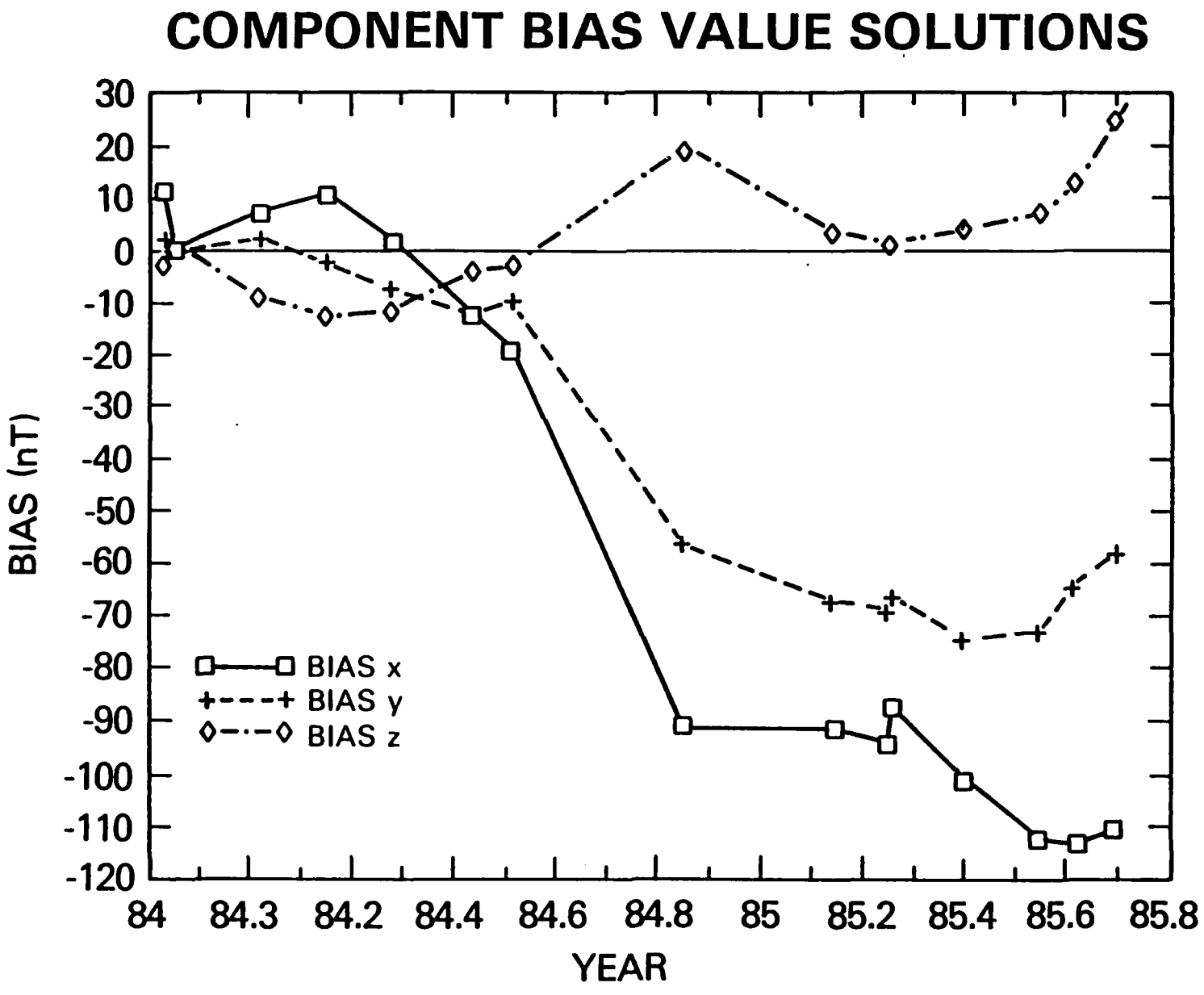
COMPONENT BIAS VALUE SOLUTIONS
BIAS (nT)
30
20
10
0
-10
-20
-30
-40
-50
-60
-70
-80
-90
-100
-110
-120
84
84.3
84.2
84.4
84.6
84.8
85
85.2
85.4
85.6
85.8
YEAR
BIAS x
BIAS y
BIAS z

Figure 7E

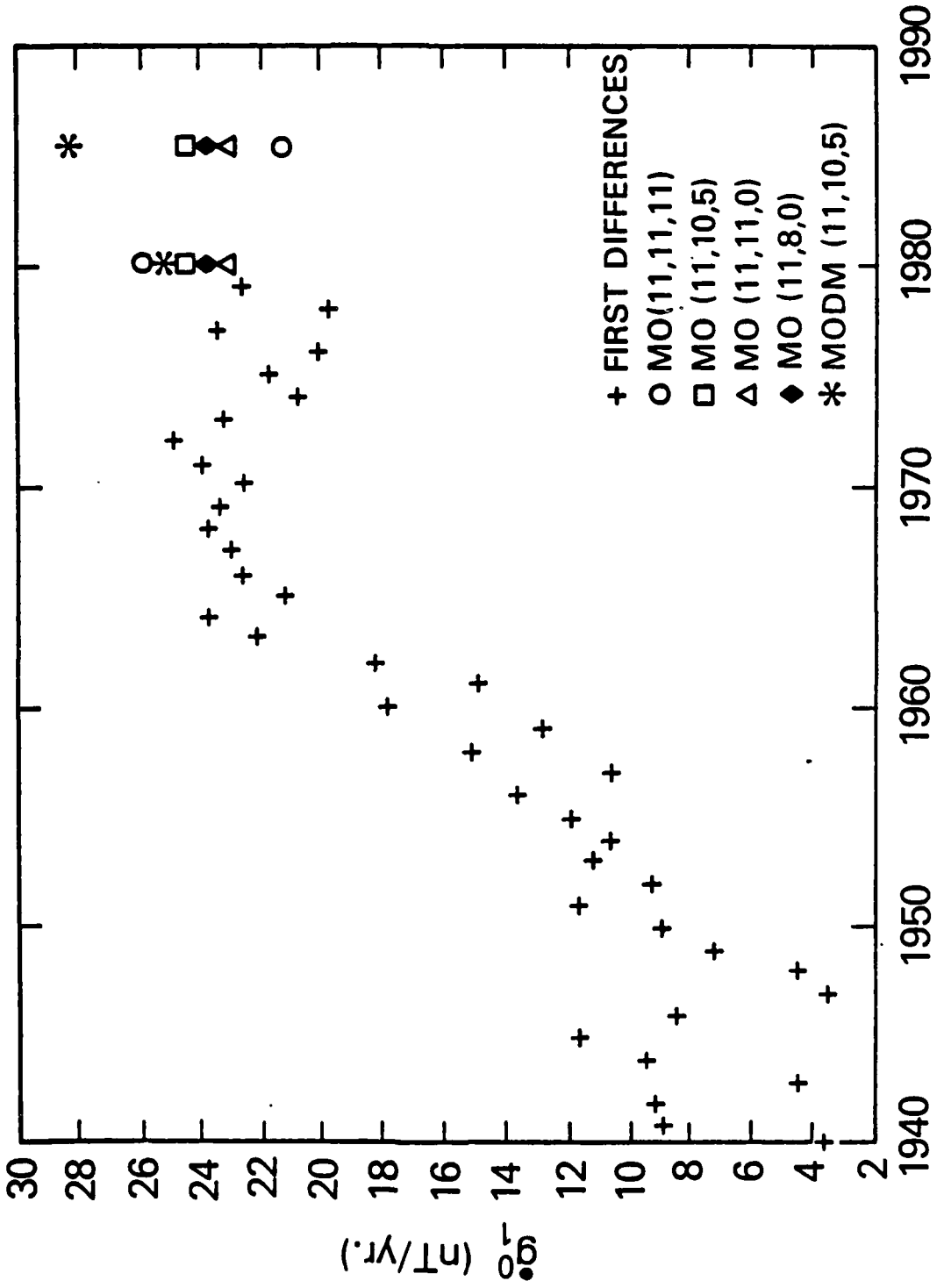
+ FIRST DIFFERENCES
○ MO(11,11,11)
□ MO (11,10,5)
△ MO (11,11,0)
◆ MO (11,8,0)
✱ MODM (11,10,5)
TIME
1940
1950
1960
1970
1980
1990
2
4
6
8
10
12
14
16
18
20
22
24
26
28
30
$\dot{g}_1^0$ (nT/yr.)

Figure 8A

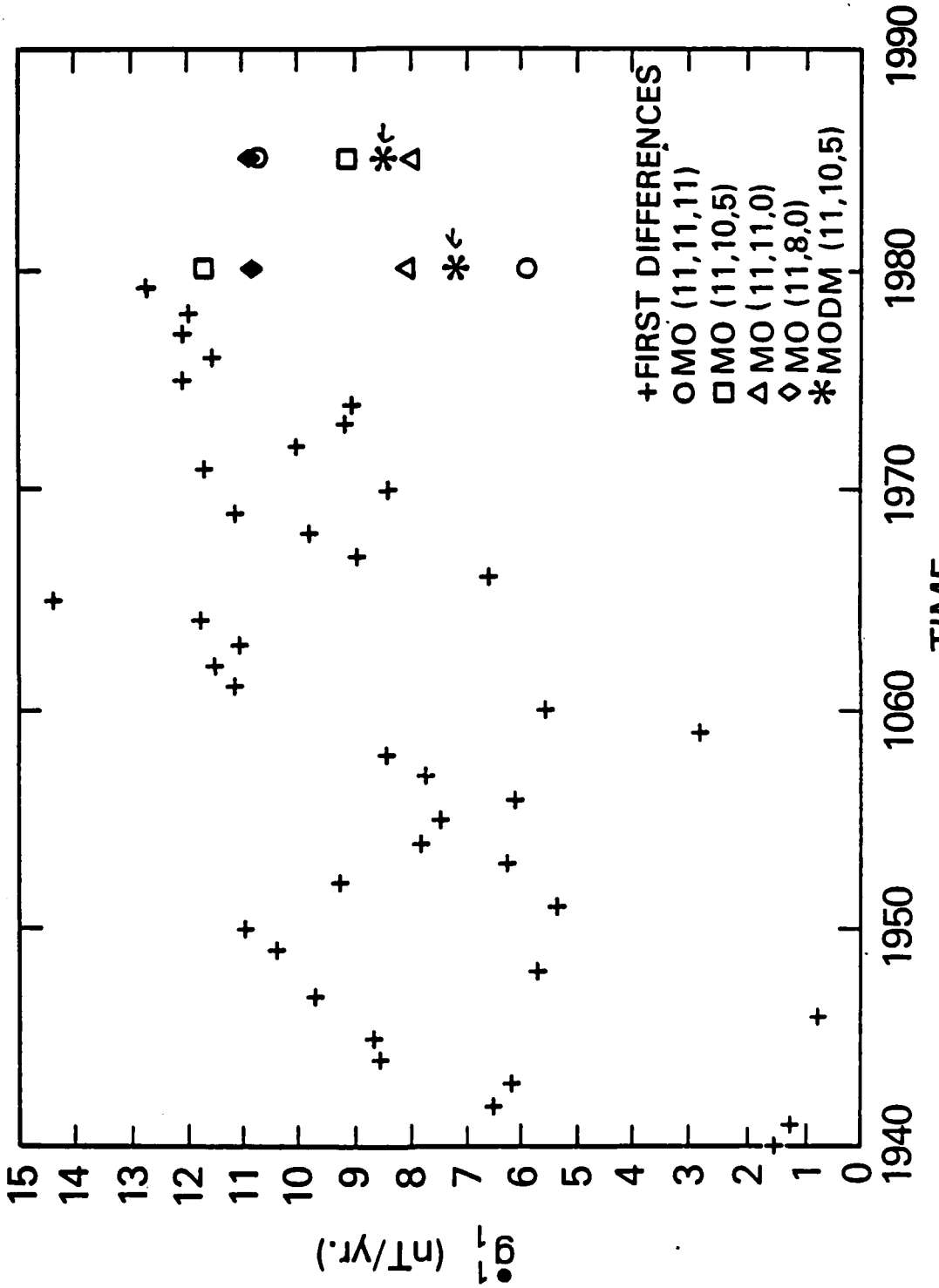
+FIRST DIFFERENCES
○MO (11,11,11)
□MO (11,10,5)
△MO (11,11,0)
◇MO (11,8,0)
*MODM (11,10,5)
TIME
1940
1950
1960
1970
1980
1990
0
1
2
3
4
5
6
7
8
9
10
11
12
13
14
15
g_1^0 (nT/yr.)

Figure 8B

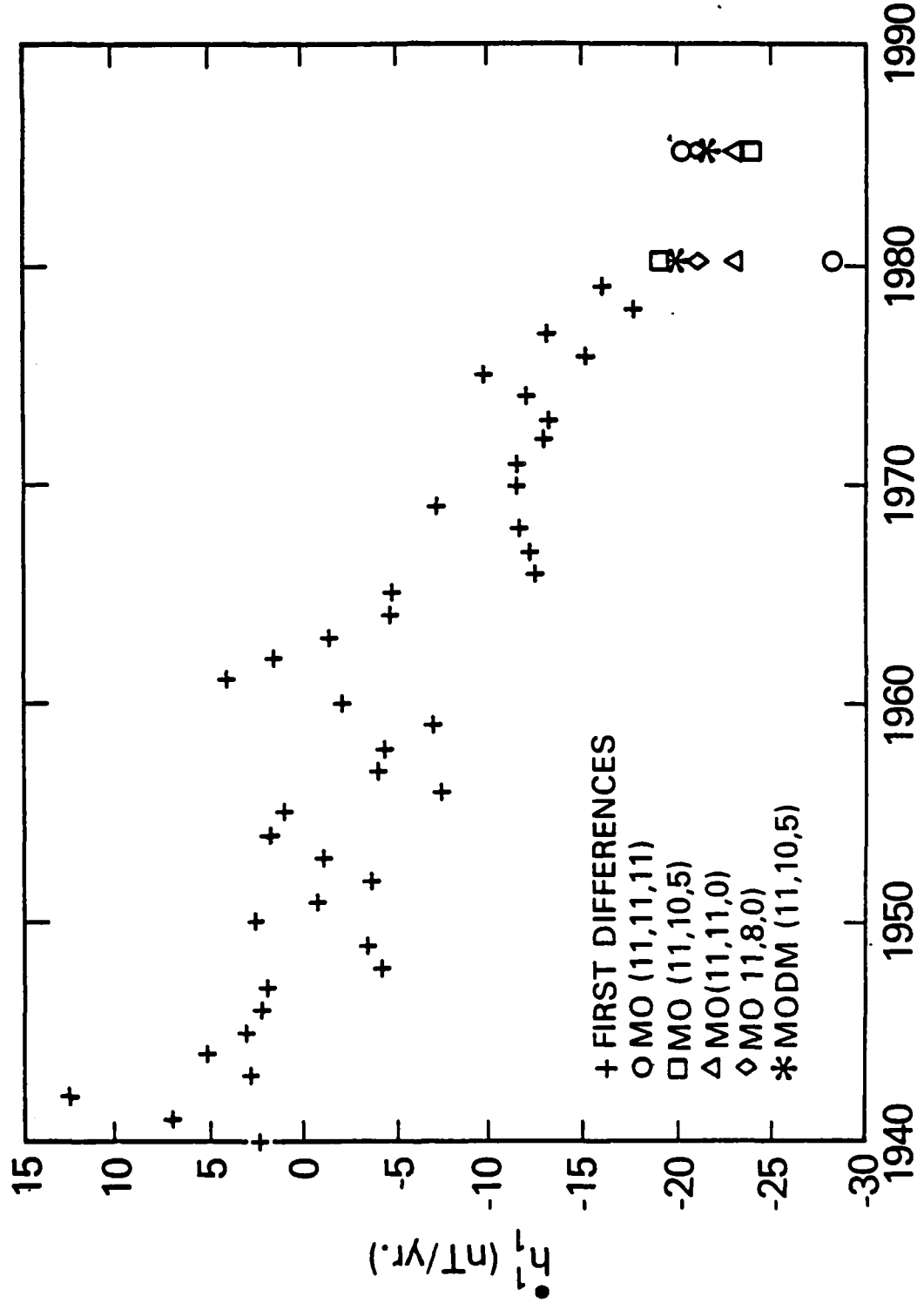
15
10
5
0
-5
-10
-15
-20
-25
-30
1940
1950
1960
1970
1980
1990
TIME
$\dot{h}_1$ (nT/yr.)
+ FIRST DIFFERENCES
○ MO (11,11,11)
□ MO (11,10,5)
△ MO(11,11,0)
◇ MO 11,8,0)
✱ MODM (11,10,5)

Figure 8C

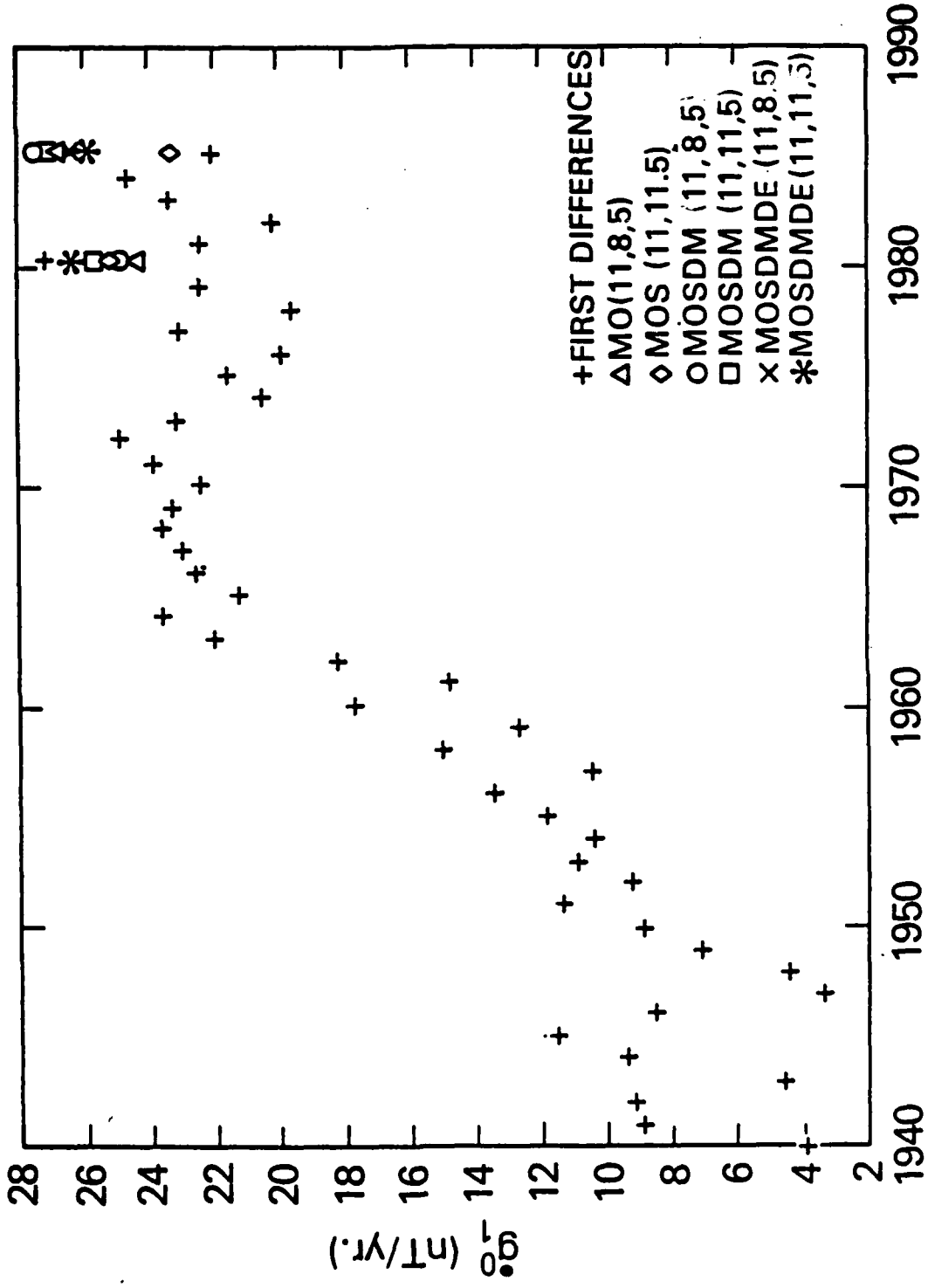
+FIRST DIFFERENCES
ΔMO(11,8,5)
◇MOS (11,11,5)
○MOSDM (11,8,5)
□MOSDM (11,11,5)
×MOSDMDE (11,8,5)
*MOSDMDE(11,11,5)
TIME
1940
1950
1960
1970
1980
1990
2
4
6
8
10
12
14
16
18
20
22
24
26
28
g_1^0 (nT/yr.)

Figure 9A

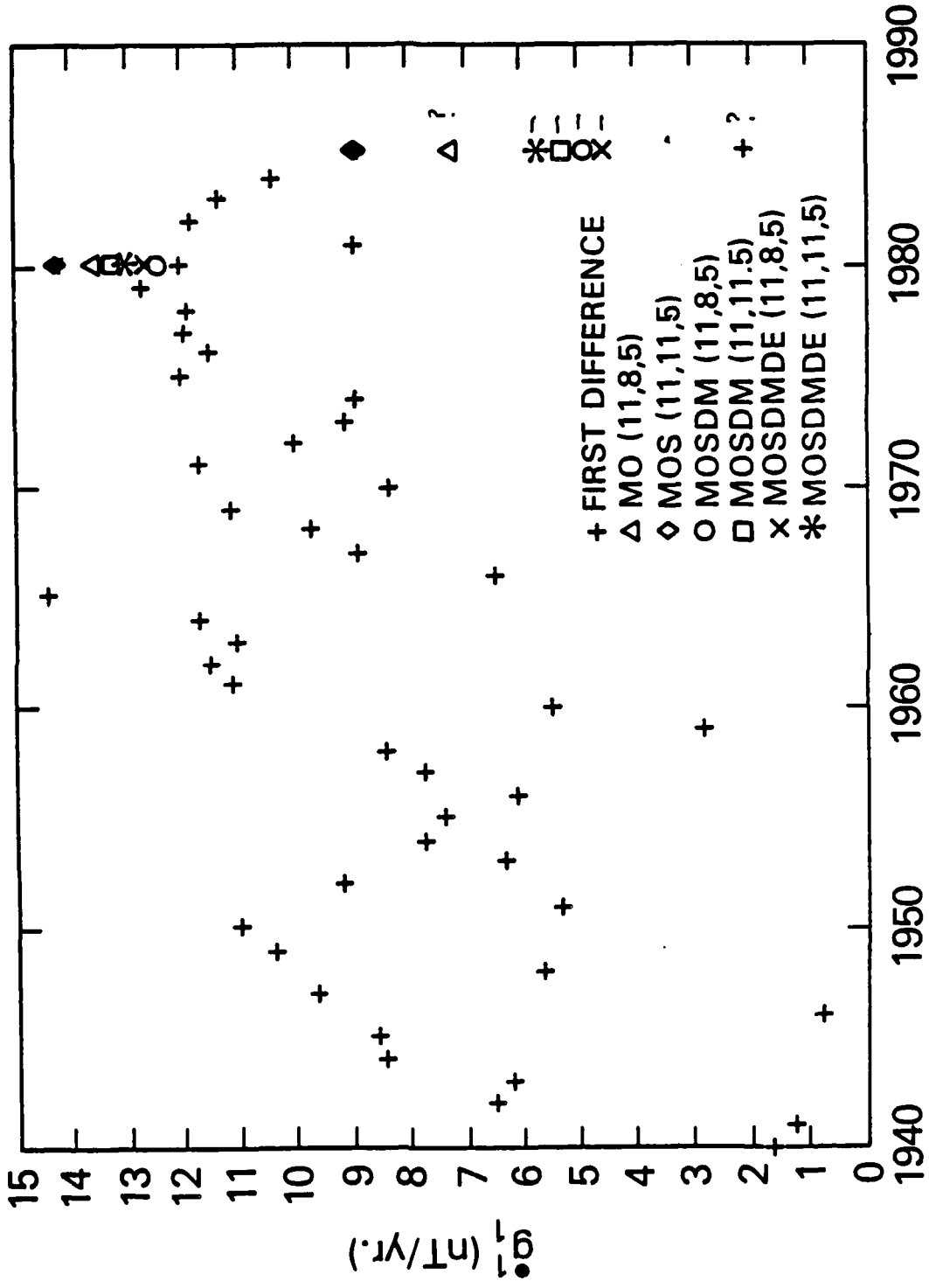
g_1^0 (nT/yr.)
TIME
+ FIRST DIFFERENCE
△ MO (11,8,5)
◇ MOS (11,11,5)
○ MOSDM (11,8,5)
□ MOSDM (11,11.5)
× MOSDMDE (11,8,5)
* MOSDMDE (11,11,5)

Figure 9B

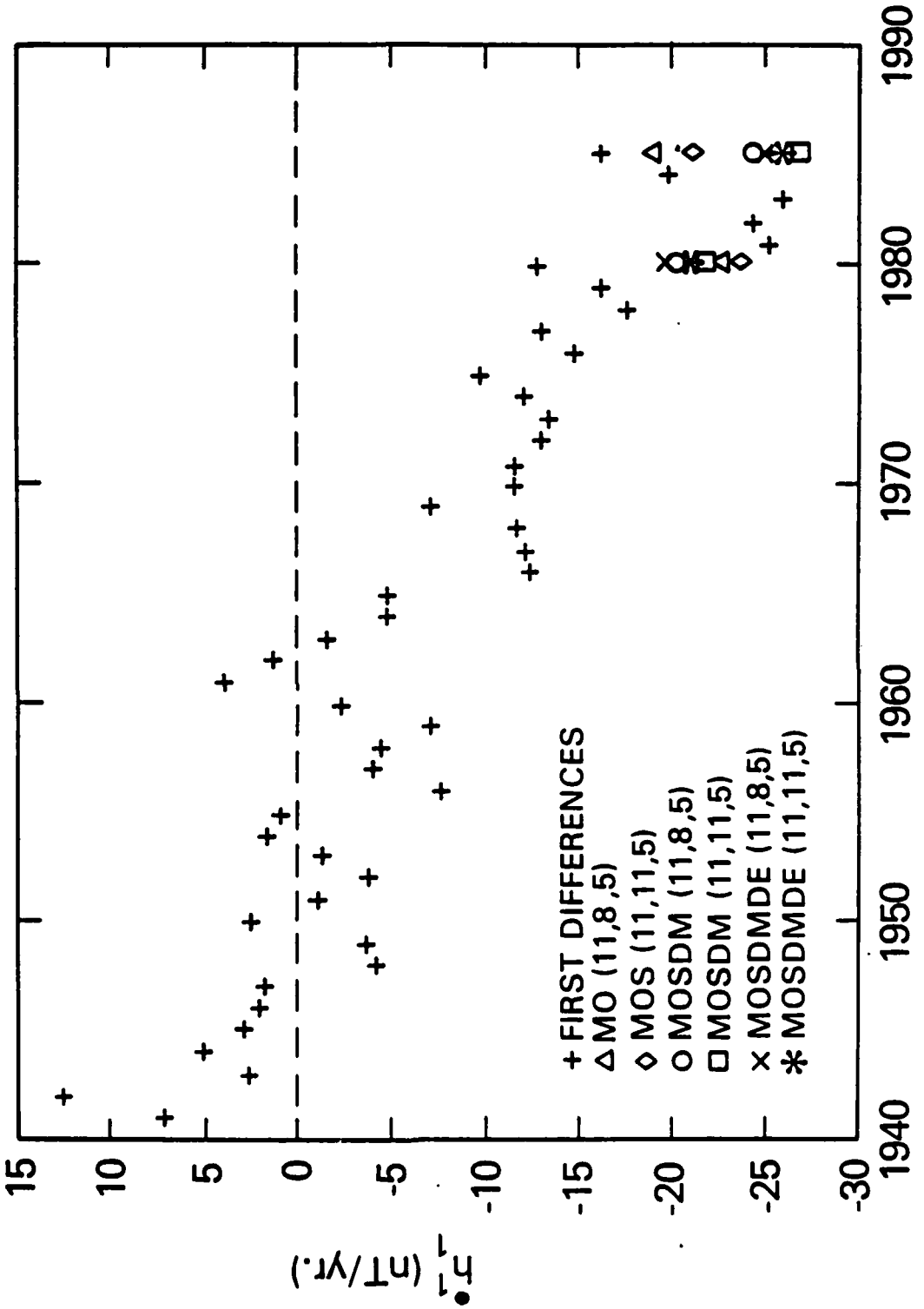
15
10
5
0
-5
-10
-15
-20
-25
-30
1940
1950
1960
1970
1980
1990
TIME
$\dot{h}_1^1$ (nT/yr.)
+ FIRST DIFFERENCES
△ MO (11,8,5)
◇ MOS (11,11,5)
○ MOSDM (11,8,5)
□ MOSDM (11,11,5)
× MOSDMDE (11,8,5)
* MOSDMDE (11,11,5)

Figure 9C

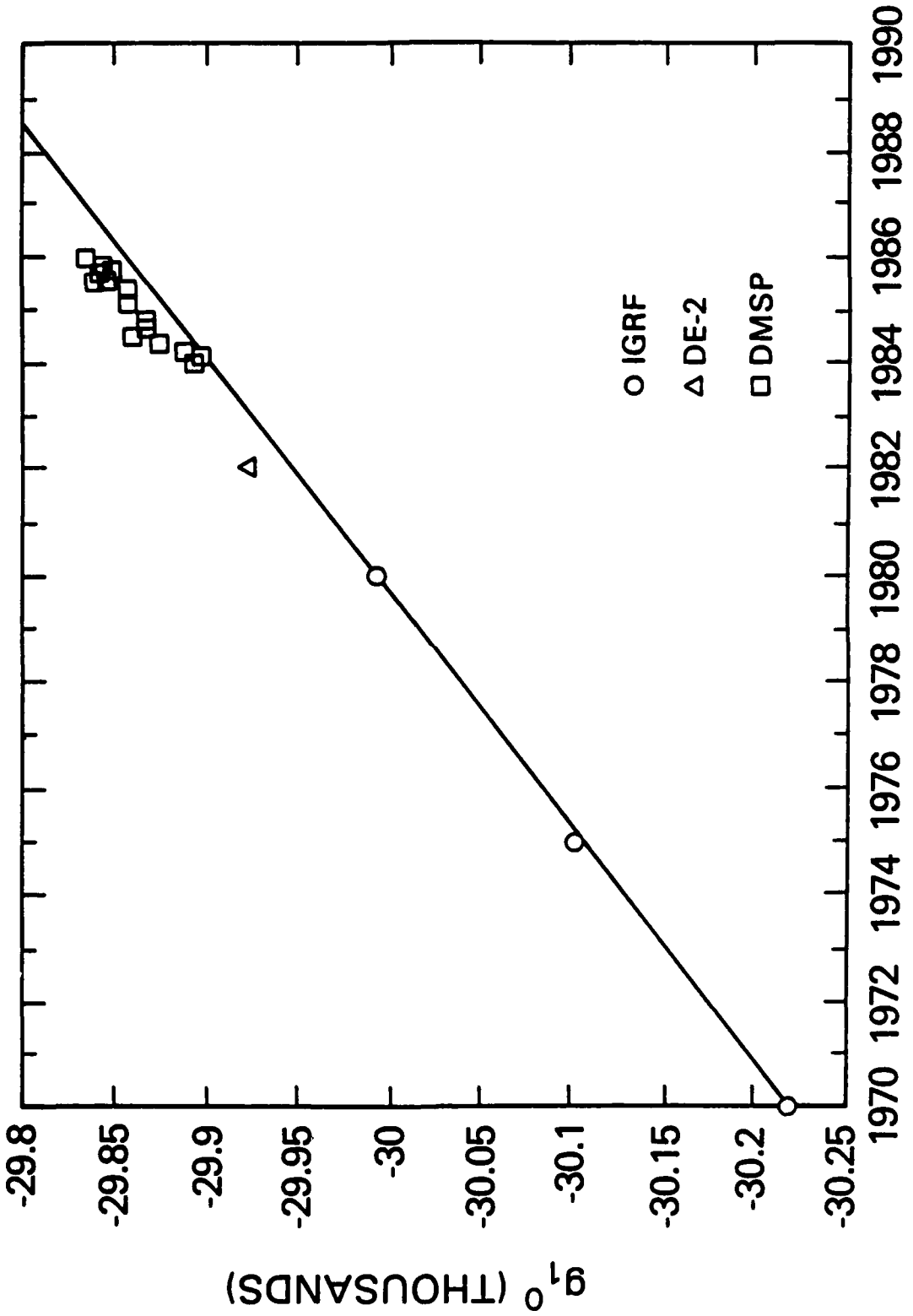
-29.8
-29.85
-29.9
-29.95
-30
-30.05
-30.1
-30.15
-30.2
-30.25
g_1^0 (THOUSANDS)
1970 1972 1974 1976 1978 1980 1982 1984 1986 1988 1990
YEAR
O IGRF
Δ DE-2
□ DMSP

Figure 10A

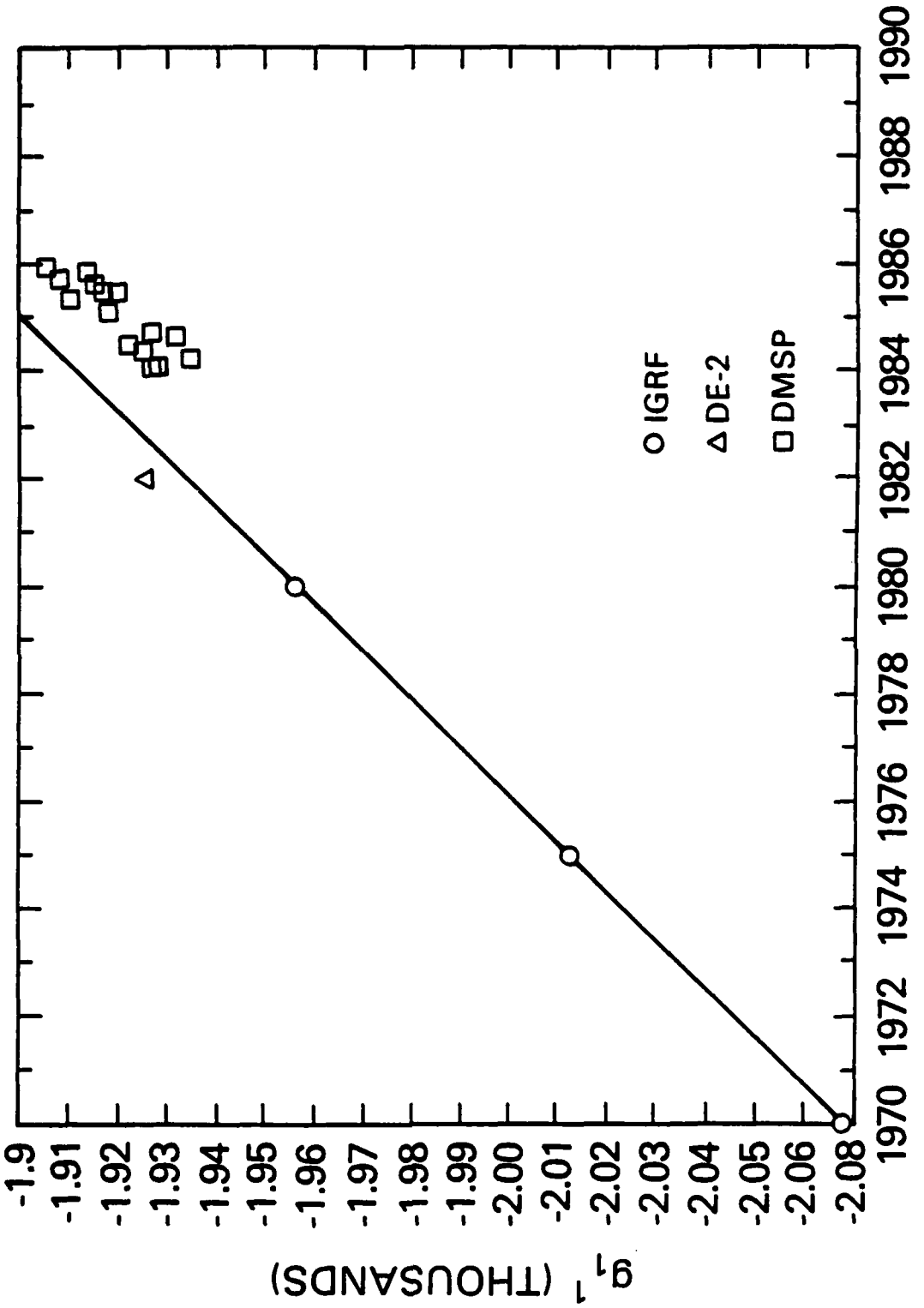
g_1^1 (THOUSANDS)
-1.9
-1.91
-1.92
-1.93
-1.94
-1.95
-1.96
-1.97
-1.98
-1.99
-2.00
-2.01
-2.02
-2.03
-2.04
-2.05
-2.06
-2.08
1970 1972 1974 1976 1978 1980 1982 1984 1986 1988 1990
O IGRF
Δ DE-2
□ DMSP

Figure 10B

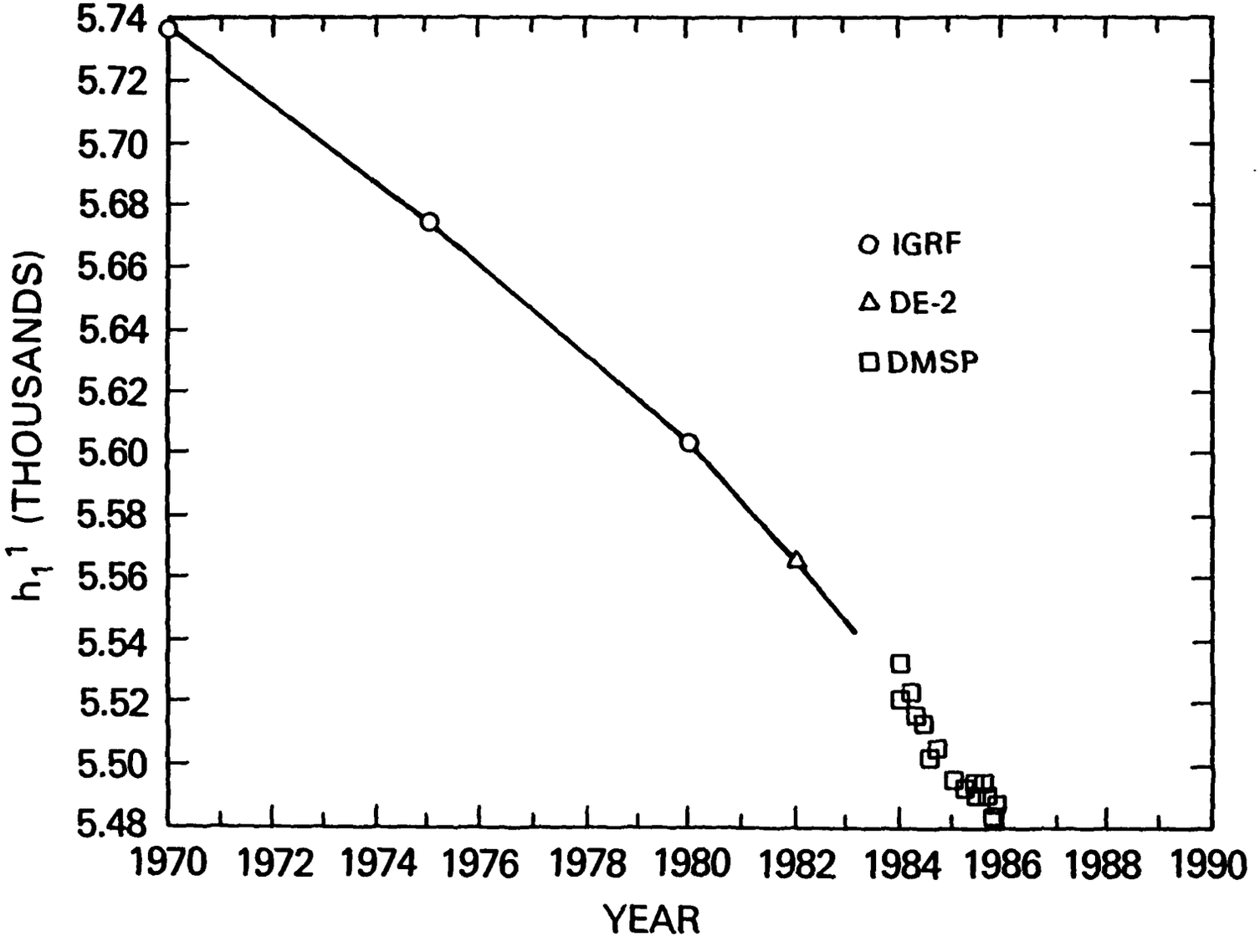
5.74
5.72
5.70
5.68
5.66
5.64
5.62
5.60
5.58
5.56
5.54
5.52
5.50
5.48
h_1^1 (THOUSANDS)
1970
1972
1974
1976
1978
1980
1982
1984
1986
1988
1990
YEAR
O IGRF
△ DE-2
□ DMSP

Figure 10C

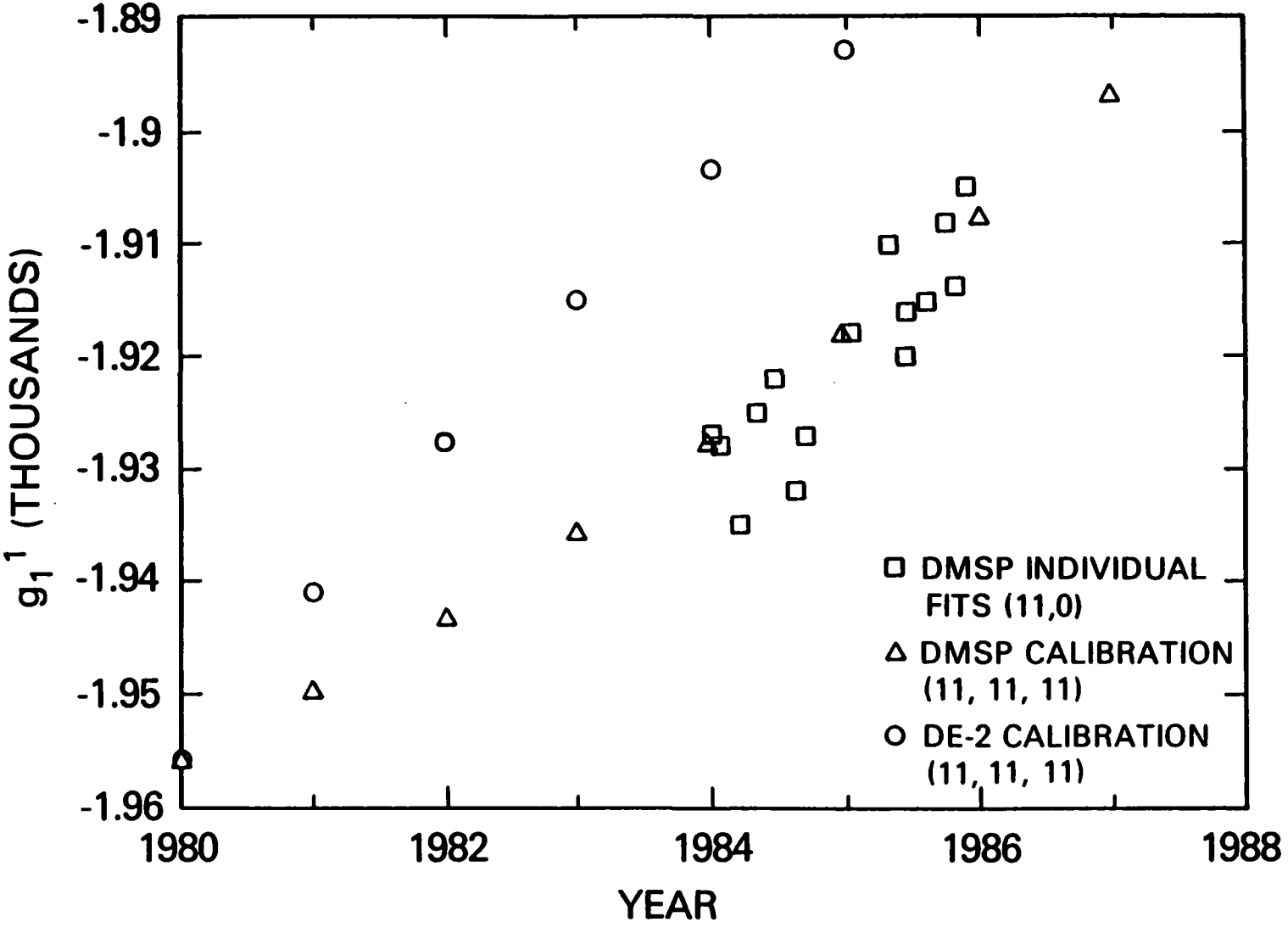
-1.89
-1.9
-1.91
-1.92
-1.93
-1.94
-1.95
-1.96
g_1^1 (THOUSANDS)
1980
1982
1984
1986
1988
YEAR
DMSP INDIVIDUAL FITS (11,0)
DMSP CALIBRATION (11, 11, 11)
DE-2 CALIBRATION (11, 11, 11)

Figure 11A

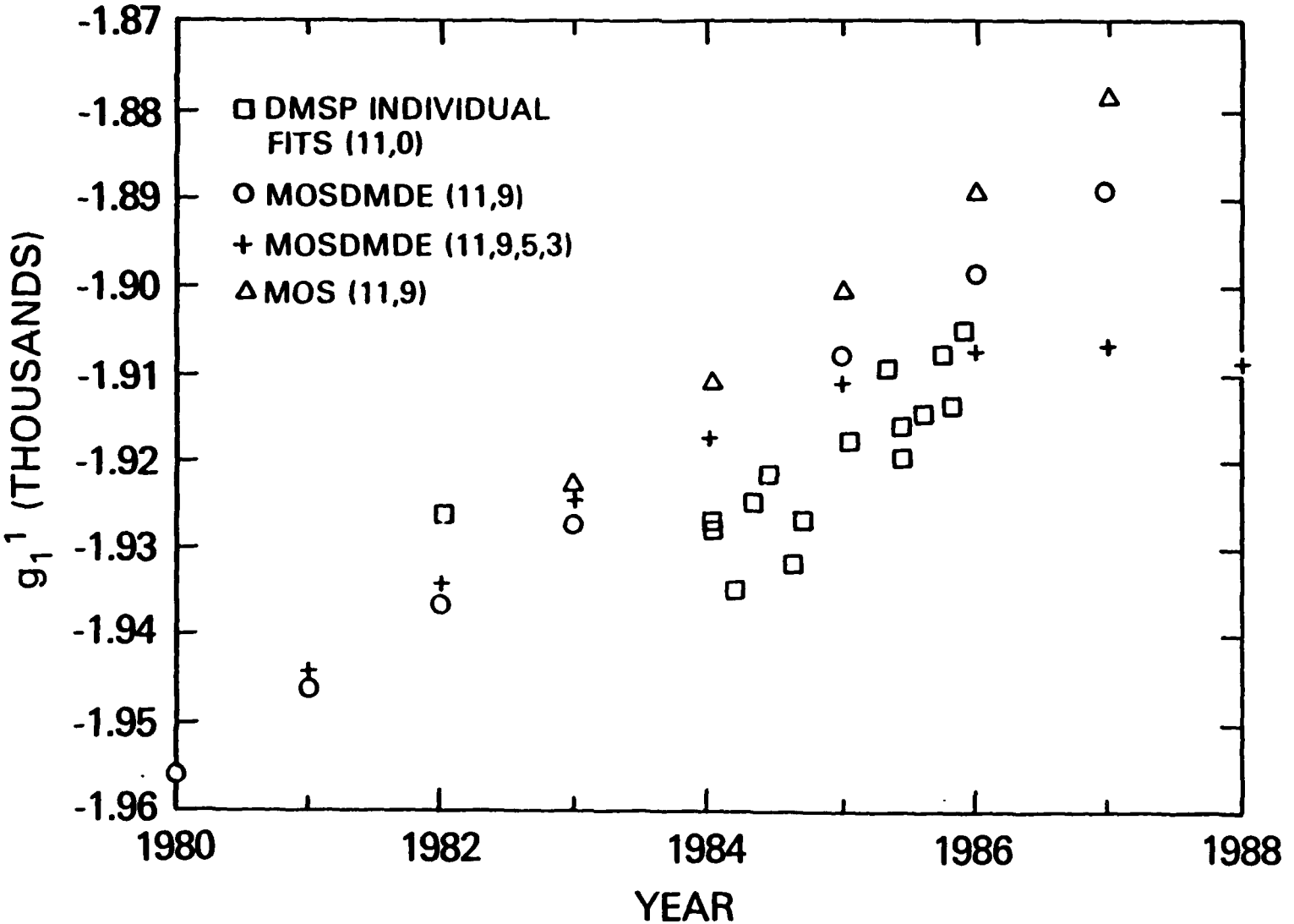
-1.87
-1.88
-1.89
-1.90
-1.91
-1.92
-1.93
-1.94
-1.95
-1.96
g_1^1 (THOUSANDS)
DMSP INDIVIDUAL FITS (11,0)
MOSDMDE (11,9)
MOSDMDE (11,9,5,3)
MOS (11,9)
1980
1982
1984
1986
1988
YEAR

Figure 11B

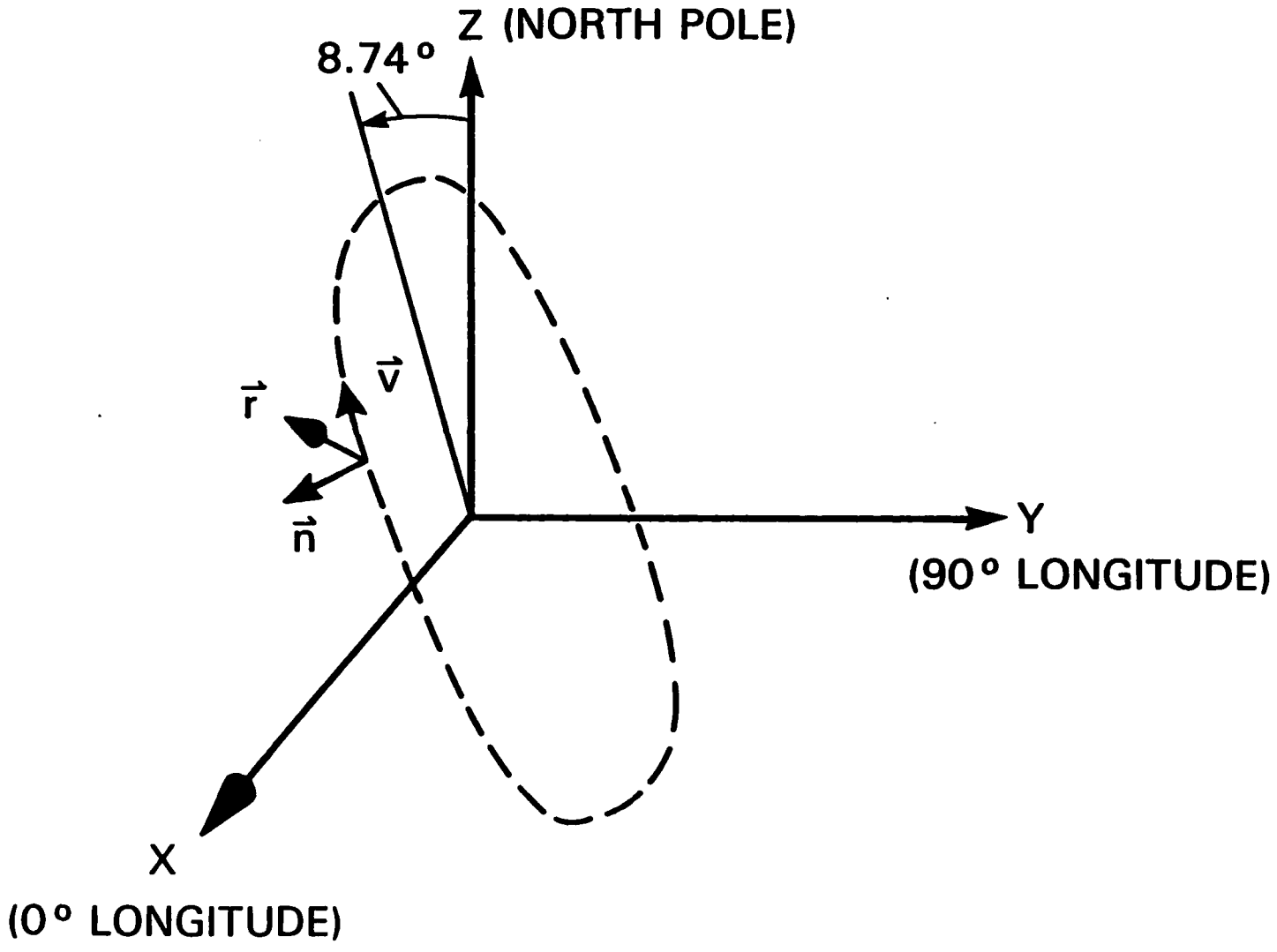

Figure B1

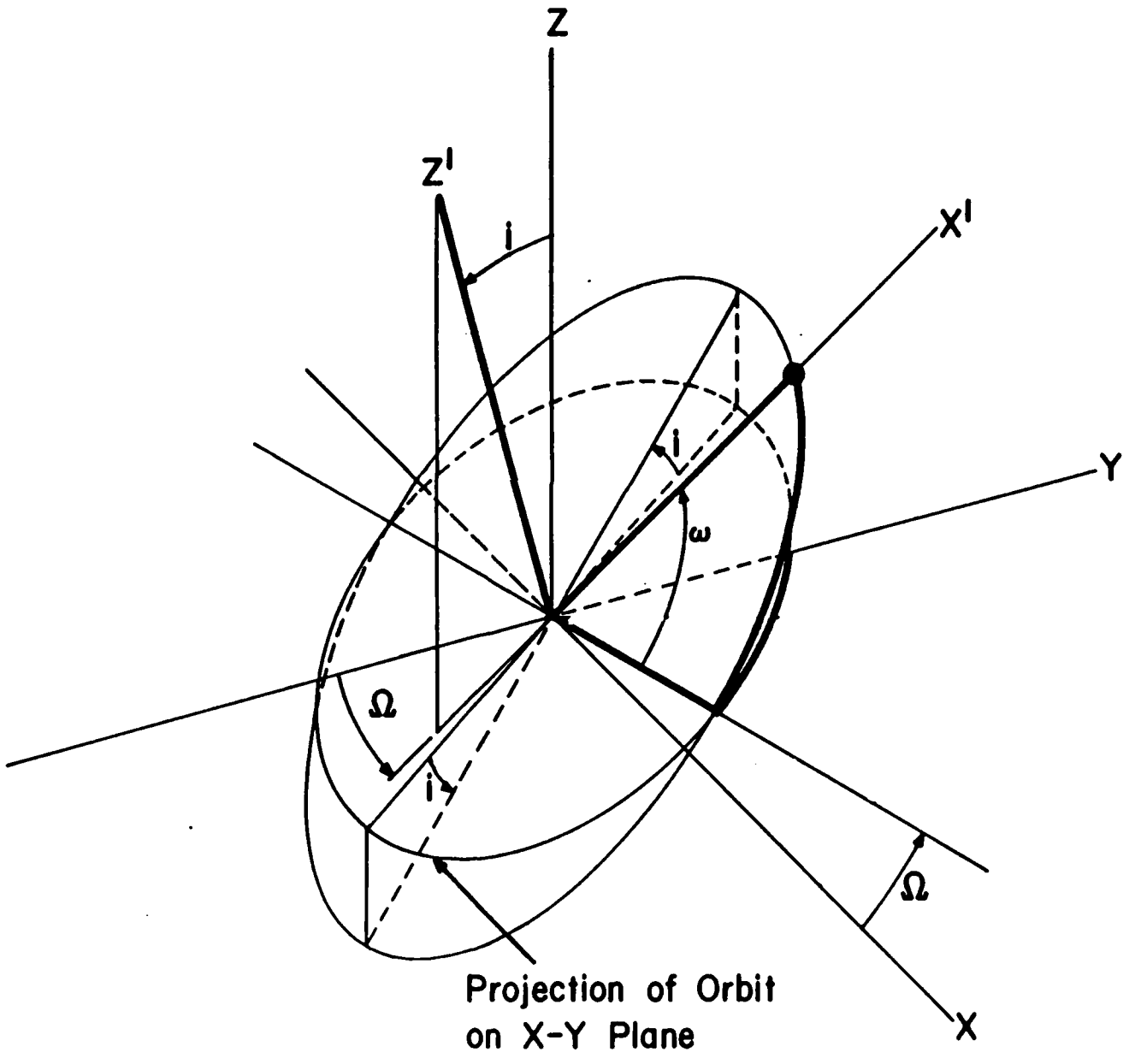

Figure B2